AD 295 095



63-2-3



295 095

DASA 1299

# EFFECTS OF SHAPE OF LOAD PULSE ON SHOCK-MITIGATING CHARACTERISTICS OF VERMICULITE CONCRETE AND A POLYURETHANE PLASTIC

by
E. F. Smith, E. S. Perry
N. Burns, J. N. Thompson

July 1962

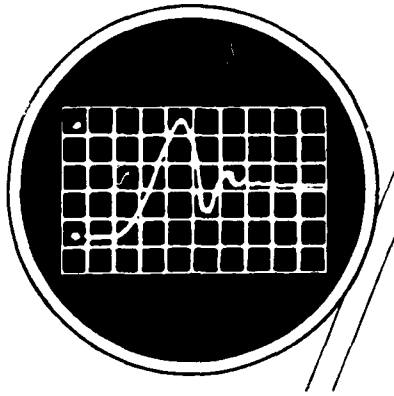

**STRUCTURAL MECHANICS RESEARCH LABORATORY**
**THE UNIVERSITY OF TEXAS**
**BALCONES RESEARCH CENTER**
**AUSTIN, TEXAS**

# EFFECTS OF SHAPE OF LOAD PULSE ON SHOCK-MITIGATING CHARACTERISTICS OF VERMICULITE CONCRETE AND A POLYURETHANE PLASTIC

by

Ervin S. Perry
Eugene F. Smith
Ned Burns
J. Neils Thompson

Prepared for

DEFENSE ATOMIC SUPPORT AGENCY
Contract DA 49-146-XZ-028
Nuclear Weapons Effects Research Number 13.040

THE UNIVERSITY OF TEXAS
STRUCTURAL MECHANICS RESEARCH LABORATORY
Austin, Texas

July 13, 1962

The Structural Mechanics Research Laboratory

is cooperatively operated by

The Engineering Mechanics and Civil Engineering Departments

at

The Balcones Research Center

University of Texas

Austin, Texas

# ERRATA

## EFFECTS OF SHAPE OF LOAD PULSE ON SHOCK-MITIGATING CHARACTERISTICS OF VERMICULITE CONCRETE AND A POLYURETHANE PLASTIC

Page 22 - Fifth line from bottom, change the word "input" to "carriage."

Page 24 - Third line, change the word "input" to "carriage."

Page 25 - Change the first paragraph under the subtitle HYGE to read as follows:

HYGE. The type of acceleration-time input pulse used in this investigation is shown by the solid line in Fig. 10. The input pulse is considered to be the pulse imparted to the cushioning material by the crushing mass and it may be considered as being a modified rectangular acceleration-time pulse. It was measured directly by an accelerometer mounted to the crushing mass which was held in the restraining frame which is initially at rest.

Page 28 - Second line, change the word "particle" to "cushioned mass."

Page 31 - Fifth line from bottom, third word from end of line, change the word "of" to "or."

Page 42 - Second line, change the words "the input" to "a carriage."

Page 43 - Thirteenth line from bottom, change the words "an input" to "a carriage."

Page 45 - Sixth and eighth lines from bottom, change the word "input" to "carriage."

Page 54 - On the left margin between the two columns of numbers, insert the words "Strain - Per Cent."

Pages 63 - 71 - Second line, change the word "input" to "carriage."

# PREFACE

This report along with the report titled Preliminary Studies of Aggregates for Shock-Isolating Lightweight Concrete constitute the final reports on Contract DA 49-146-XZ-028. This contract provided for a feasibility study and an experimental study of materials and systems for the isolation of underground structures subjected to dynamic loads.

Two previous reports under this contract have been issued:

> Dynamic Energy-Absorbing Characteristics of Lightweight Vermiculite Concrete by Clarke Covington, June 1961.
>
> Shock Mitigation with Lightweight Vermiculite Concrete by Richard Shield, Ervin S. Perry, E. A. Ripperger, and J. Neils Thompson, February 1962.

These reports explored the potential of high-air-content, lightweight vermiculite concrete as a shock mitigator or shock isolator. The rate of deformation and the resulting effects on the stress-strain characteristics were studied particularly.

Because of the uncertain shape of load pulse imparted to an underground structure subjected to blast-type loadings, it was considered necessary to investigate the effect of the shape of load pulse, as obtained from different methods of dynamic testing, on the stress-strain characteristics of the material. This investigation is a continuation of the two previous studies with one additional material, a polyurethane plastic, added.

A Hyge Shock Tester was used to impart dynamic loads to the material. This technique was studied in an effort to establish an experimental procedure for measuring the effectiveness of shock-mitigating

or shock-isolating materials. Versatility of this technique will enable extension of studies and expedite the evaluation of materials through a wide range of impact conditions.

The investigation reported herein provides substantial evidence of the feasibility of utilizing vermiculite concrete and a polyurethane plastic as a dissipator of energy to enable shock mitigation. Other materials undoubtedly can be used for this same purpose providing environmental conditions are compatible with the maintenance of the physical and mechanical properties of the material.

As a special assignment under this contract, the Structural Mechanics Research Laboratory made an investigation and issued the following report:

Analysis of Structural Damage from the 1960 Tsunami at Hilo, Hawaii.

Directing Staff:

J. Neils Thompson, Director and Professor of Civil Engineering

E. A. Ripperger, Associate Director and Professor of Engineering Mechanics

Hudson Matlock, Associate Director and Associate Professor of Civil Engineering

Lymon C. Reese, Associate Director and Associate Professor of Civil Engineering

Ned Burns, Research Engineer (Faculty), and Assistant Professor of Civil Engineering

Eugene F. Smith, Research Engineer (Faculty), and Instructor of Civil Engineering

Ervin S. Perry, Research Engineer Assistant III.

Robert Matlock, Research Engineer IV.

Robert I. Carr, Research Engineer I.

J. Neils Thompson, Director
Structural Mechanics Research Laboratory
The University of Texas
Austin, Texas

July 13, 1962

TABLE OF CONTENTS

TABLE OF CONTENTS
(Cont'd)

TABLE OF CONTENTS

(Cont'd)

## LIST OF FIGURES AND TABLES

LIST OF FIGURES AND TABLES
(Cont'd)

## LIST OF FIGURES AND TABLES
(Cont'd)

## ABSTRACT

Preliminary indications of the effects of load pulse on the shock-mitigating characteristics of lightweight vermiculite concrete and a polyurethane plastic are presented. Different input load pulses were obtained in tests on these materials using three different methods of dynamic testing. In the current study, a HYGE Shock Tester was used to provide the impact energy. The form of the characteristic acceleration-time curve from this study is compared with the form of those obtained in previously reported tests using air gun and drop tower facilities.

Stress-strain curves obtained from the three different types of tests were found, in general, to be similar in some respects. Important differences were noted, however, and an attempt is made to explain them in terms of basic differences in the testing methods utilized.

Reduction of the test data was facilitated by the use of both analog and digital computers. A brief description of the two methods of data reduction is given. Stress-strain curves from the two methods are compared to indicate their similarity.

# INTRODUCTION

## Background

This report is the third in a series to explore the potential of high-air-content, lightweight concrete with low-strength aggregate and polyurethane foamed plastic as shock mitigators or shock isolators. Two previous studies* [1, 2] of lightweight concrete using vermiculite aggregate have been reported.

In the first study,[1] the dynamic energy-absorbing characteristics of confined lightweight vermiculite concrete (hereinafter referred to in this report as vermiculite concrete) were investigated by analyzing stress-strain and stress-time relationships made under varying conditions. Those conditions were principally variable mass weight and variable impact velocities, from 10.8 to 60 fps, with the input energy held constant. The impact energy was provided by a freely falling mass, using the Structural Mechanics Research Laboratory's 275-ft drop tower, for which the force-sensing device was a fixed force plate supported by four dynamometers.

In the second study,[2] the energy-absorbing characteristics of the same material were investigated by a different technique. The variable conditions were higher impact velocities, from 24 to 120 fps, than were obtained by using the drop tower, and variable specimen thickness. The impact energy was provided by a projectile fired from a 4-in.-bore compressed air gun. The measuring technique used was a variation of

---

*Numbers indicate references as listed in the Bibliography.

the one used at the drop tower, with the essential difference being that the force-sensing device, an accelerometer, was permitted to move.

In this study, a high-impact HYGE Shock Tester (hereafter referred to in this report as the HYGE) was used to provide a means for varying the carriage accelerations imparted to the cushioning specimens. It is capable of producing thrust loads up to 40,000 lb and carriage acceleration values to several hundred times gravity for milliseconds duration of time. The force-sensing devices, similar to that in the second study, were accelerometers that moved with the specimen and carriage. A more detailed explanation will be given later in this report.

## Objectives

This investigation supplements the previous studies of the energy-absorbing characteristics of vermiculite concrete [1, 2] and of polyurethane foamed plastics. [3]

The objectives of this study were threefold:

1. Develop procedures and analyzing techniques for evaluating the characteristics of materials loaded by the HYGE
2. Compare and correlate results from the HYGE with the results obtained in the previous studies with the air gun, drop tower, and static testing facilities
3. Summarize the configurations of the stress-strain curves and the input pulses imparted to the cushioning material by the three dynamic methods and the static test.

## Scope

This report is concerned with the effect of the configuration of the acceleration-time input pulses produced by three different test methods on shock-mitigating characteristics of certain materials. Only one shape of the carriage acceleration-time pulse, a modified square, was used for the HYGE. Other configurations of the carriage acceleration-time pulse can be secured by changing metering pins in the HYGE.

It is anticipated that, in the future, more extensive work will be performed on the effects of the load input pulse parameters, particularly with the HYGE.

## EXPERIMENTAL PROGRAM

### Scope

A limited number of tests were conducted on the HYGE using vermiculite concrete and a polyurethane foamed plastic. These cushioning materials were chosen to take advantage of results obtained in previous studies,[1, 2, 3] and to further investigate their dynamic energy-absorbing characteristics as they are affected by the input energy supplied by a different dynamic method.

Figure 1 shows the major features of the HYGE. Acceleration of the carriage is produced by a differential gas pressure acting on two faces of a thrust piston and column assembly on which the carriage rests. By recording the response of accelerometers located on the carriage and on a mass resting on the material being tested, the forces and deformations developed during crushing of the cushioning material can be determined.

A series of acceleration-time measurements for the carriage and crushing mass were made with two variable conditions. They were:

1. Variation in carriage accelerations from 61 to 125g for vermiculite concrete, and from 42 to 114g for foamed plastic
2. Variation of weight of the crushing mass from 70.6 to 126.7 lb for vermiculite concrete, and from 49.5 to 154.2 lb for foamed plastic.

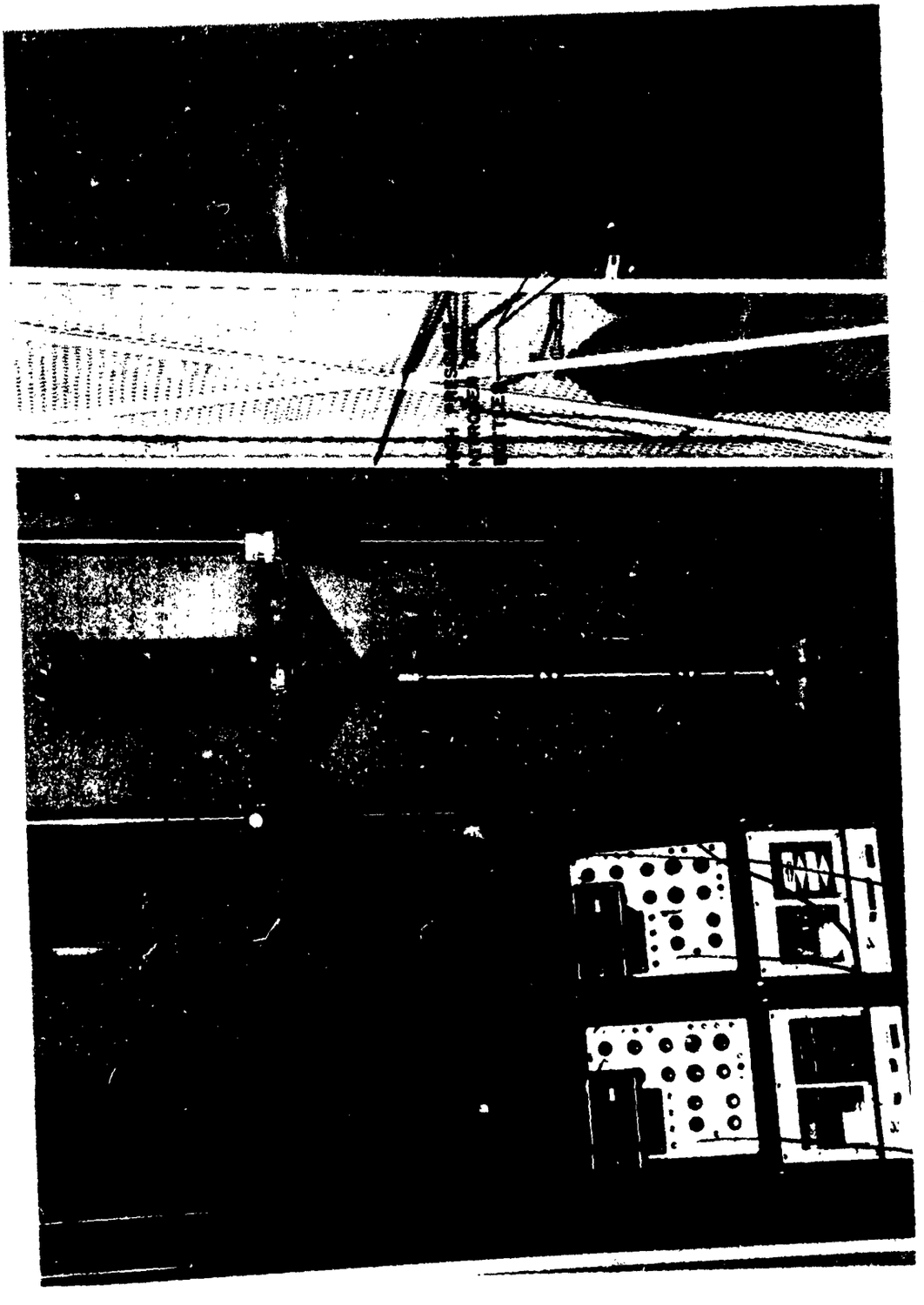

Fig. 1. Over-All View of HYGE Shock Tester and Apparatus

## Description of Materials

Vermiculite. Vermiculite is a lamellar micaceous material that contains combined water. When the raw material is subjected to quick heating to the softening temperature, the material puffs because of the conversion of the contained water into steam. This produces an expanded aggregate that has a relatively low density and a high water-absorption property. The vermiculite used in this investigation was Zonolite Plaster Aggregate No. 3. It is sold commercially by the Texas Vermiculite Corporation of Dallas, Texas. The No. 3 vermiculite aggregate has a density of 7 to 10 lb per cu ft loose volume, and is sized so that virtually all of the material passes a No. 8 sieve. All of it is retained on a No. 30 sieve.[1]

Cement. Type III (High-Early-Strength) portland cement, manufactured by the Alamo Cement Company of San Antonio, Texas, was used in the preparation of the vermiculite concrete. Portland cement weighs 94 lb per cu foot.

Admixture. A neutralized vinsol resin, made by the Hercules Powder Company, was used as an air-entraining agent in the mix to produce a more plastic mix.

Foamed Plastic. The foamed plastic used in this program was Quartermaster polyurethane-plastic 108C. The material was supplied by the Quartermaster Research and Engineering Command at Natick, Massachusetts. It was fabricated by the Atlantic Research Corporation of Alexandria, Virginia, and was used in a previous study.[3]

## Production of Vermiculite Concrete

Mix proportions. The vermiculite concrete investigated was

mixed with the following proportions per batch to conform to the mix proportions used in previous studies:[1, 2]

| | |
|---|---|
| Expanded vermiculite aggregate | - 2 cu ft |
| Type III portland cement | - 0.25 cu ft |
| Water | - 0.77 cu ft |
| Admixture (AEA) | - 100 gm |

This mix gave a cement-to-aggregate ratio of one-to-eight by volume.[2]

Mixing procedure. The procedure for preparing the specimens consisted of (1) thoroughly mixing all of the admixture with the mixing water in a separate container; (2) placing all of the aggregate and 20 pounds of water and admixture in the mixer, and mixing for 3 minutes; (3) placing all of the cement into the mixer, and mixing for 3 minutes; and (4) placing the remainder of the water into the mixer, and mixing for 7 minutes. This procedure resulted in a uniform concrete with approximately 8-in. slump, an air content between 25 and 30 per cent, and a unit weight of approximately 50 lb per cu foot.[2]

A horizontal Lancaster mixer was used in preparing the vermiculite concrete specimens.

Curing. Specimens were poured in standard 6 x 12-in. steel cylindrical molds, and were cured in the molds for 2 days. After removal from the molds, the specimens were immediately sealed in plastic bags to prevent evaporation of the mixing water. They were stored in this condition at a temperature of about 72F until tested. Identical specimens may be seen in their sealed plastic bags in Fig. 2

of Ref. 2. The ages of the test specimens varied from 82 to 95 days.

## Preparation of Specimens

Vermiculite concrete. On removing the vermiculite concrete specimens from their sealed plastic bags, they were easily sawed by a hacksaw to the required 6-in. specimen height. Their end faces were scraped until plane to insure uniform distribution of the crushing mass force over the impact area. Each specimen was very uniform in appearance and nature, and weighed slightly less than 5 pounds. Each specimen was immediately tested after being cut and shaped in order to reduce the effect of moisture evaporation from the specimen.

Figure 2 shows a typical vermiculite concrete test specimen.

Foamed plastic. The foamed plastic specimens were prepared by cutting 24 x 24 x 6-in. pads into cylindrical specimens 6-in. in diameter and 5-1/4-in. in height. This was executed readily by using a band saw. The specimens were cut from material that had a bulk density of 6 lb per cu foot.

The major portion of each specimen was very uniform in appearance and nature. Each specimen did, however, possess some large holes, which can be observed in the specimen shown in Fig. 3. These holes undoubtedly contributed to the variation in the results obtained in the HYGE tests.

## Instrumentation

HYGE shock tester. Basically, the HYGE, as diagrammed in Fig. 4, consists of a closed cylinder which is separated into two

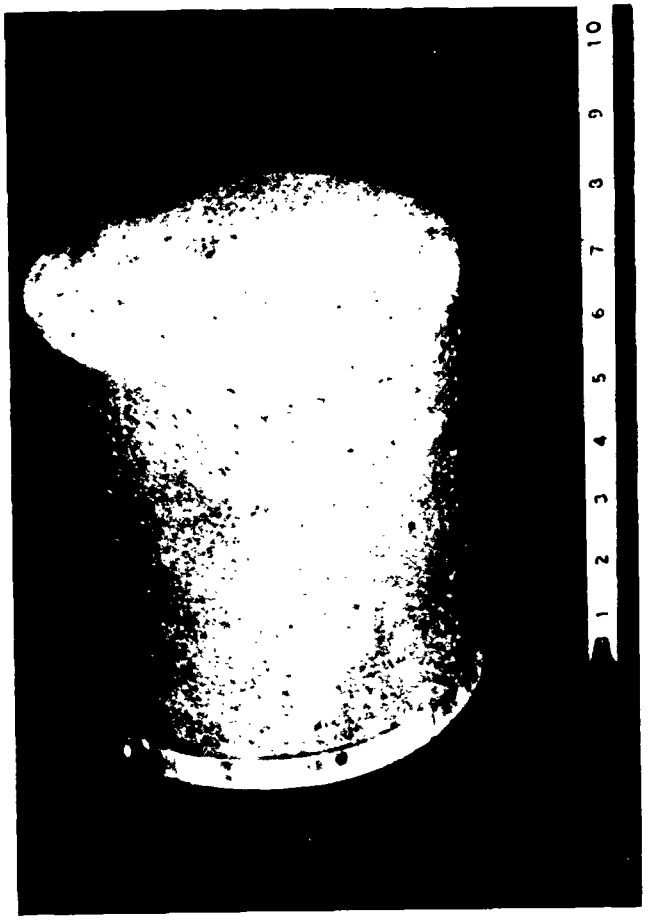

Fig. 2. Vermiculite Concrete Specimen Before Crushing

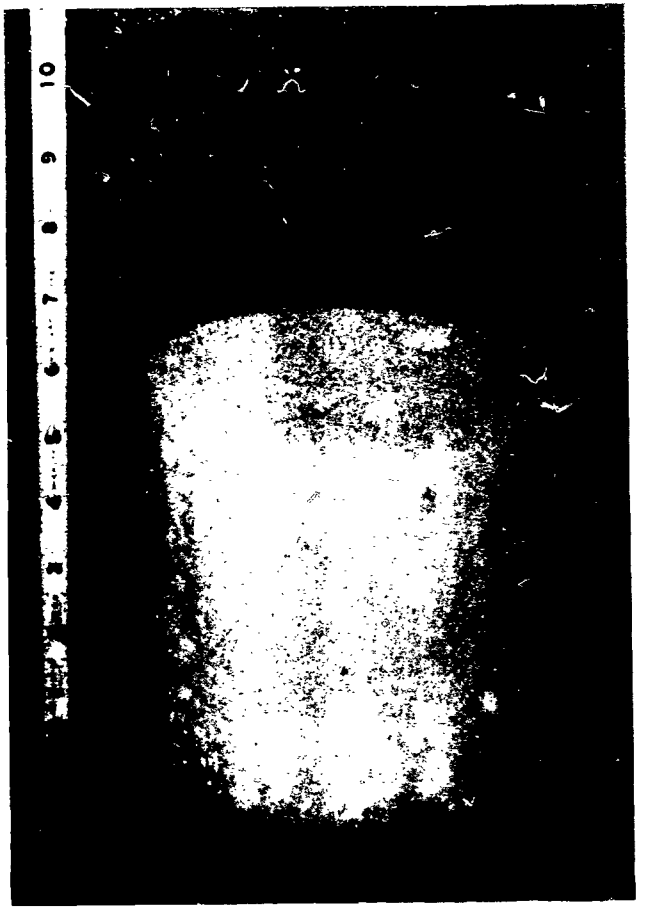

Fig. 3. Foamed Plastic Specimen Before Crushing

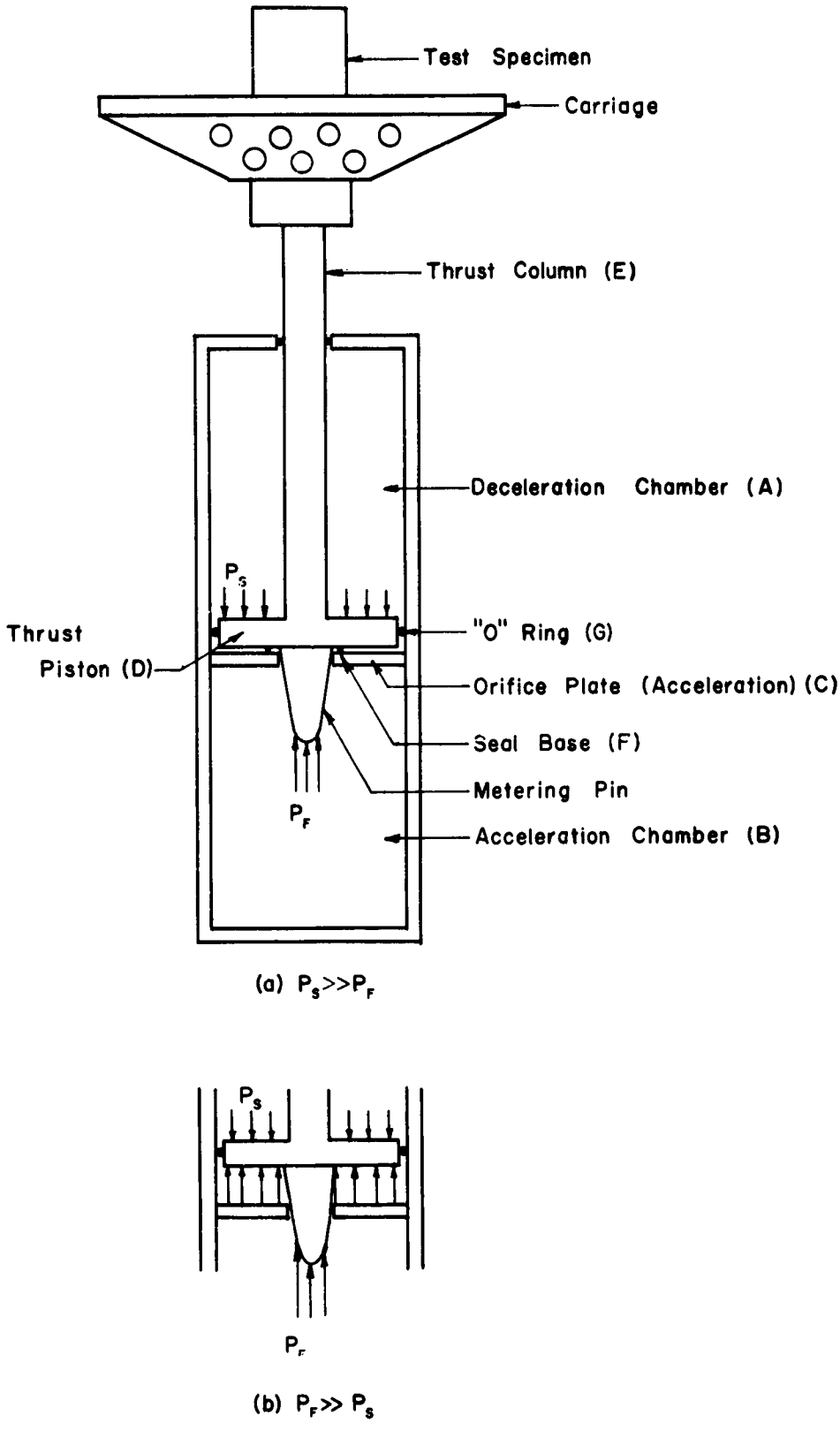


Fig. 4. Principle of Operation of HYGE Shock Tester.[4]

chambers, a deceleration chamber (A), and an acceleration chamber (B), by an orifice plate, (C). A thrust is developed through differential gas pressures acting on the two faces of a thrust piston, (D). It is transmitted from the cylinder to the thrust assembly, consisting of the thrust piston and thrust column (E), and then to the carriage and test specimen which rests on the carriage.

To prepare for firing, a relatively low set pressure ($p_s$) is introduced into the deceleration chamber from compressed nitrogen gas bottles. This forces the thrust piston against a seal ring (F), seated on top of the orifice plate. The proper carriage brake pressure (predetermined before firing for specific test conditions) is then set to limit vertical movement of the carriage and test specimen. After this has been done, the operator then introduces the predetermined load or firing pressure ($p_f$) into the acceleration chamber. Since the force exerted on the thrust piston by the load pressure is greater than the force exerted by the set pressure, the seal at the orifice is opened and causes the thrust piston to rise. The entire bottom area of the thrust piston is almost instantly exposed to the load pressure from the acceleration chamber. The metering pin, which is connected to the lower end of the thrust column, controls the flow of gas from the acceleration chamber to the deceleration chamber. The shape of the carriage acceleration-time pulse is controlled by the shape of the metering pin used. The limited-duration thrust is transmitted by the thrust column to the carriage upon which the specimen is mounted, thus imparting an instantaneous upward acceleration to the carriage

and test specimen. These are accelerated vertically a distance of several feet along the 20-ft rail system.

If a mass is mounted on top of the test specimen, the acceleration of the mass will exert a force on the specimen causing it to be crushed. Acceleration-vs-time measurements are recorded for both the carriage and crushing mass by the other instrumentation, from which a stress-strain curve of the cushioning material may ultimately be obtained.

After firing, the load pressure is "bled" into the nitrogen gas bottles, and the set pressure is reduced slightly. The carriage and specimen are then carefully brought down, so that the carriage once again rests on the thrust column.

Restraining frame. The restraining frame is shown in Fig. 5. In preparation for firing, the test specimen is placed inside its confining vessel and these, in turn, are placed inside the frame and rested on the carriage. A 4-in.-diameter, solid steel, nonvariable mass is placed on the specimen. Brass discs are placed on top of the nonvariable mass. The crushing mass is varied by changing the number of discs.

The restraining frame serves the double purpose of restraining the cushioning specimen from lateral movement and of guiding the crushing mass during a test. As crushing of the specimen takes place, differential movement between the crushing mass and restraining frame occurs. Friction forces acting between the crushing mass and restraining frame are definitely small. It is believed that the friction forces are negligible because of the clearance between the crushing mass and


Fig. 5. Restraining Frame and Accelerometer Arrangement

restraining frame.

Accelerometers. An accelerometer is mounted rigidly to the carriage to measure the acceleration imparted to the mass-cushion system. Another accelerometer, protected by two wooden blocks, is bolted to the top disc of the crushing mass. It measures the acceleration transmitted through the cushion system. Several rubber pads are then inserted on top of the arrangement to further protect the crushing mass accelerometer and to cushion the crushing mass during the deceleration stage. The arrangement is shown in Fig. 5.

Statham Model A5-500-350 accelerometers, having an operating range of $\pm$500g, a natural frequency of approximately 2000 cps, and a damping factor of approximately 0.60 of the critical value, are used throughout the test program.

Theoretical response curves for an accelerometer are given in Appendix B of Ref. 2. These previously calculated curves indicate for the type of pulse studied, maximum overshoot may vary from 2 to 10 per cent depending on the damping. For the particular accelerometer used, the accelerometer can be expected to overshoot by about 6 per cent when the rise time of the acceleration pulse is about one-tenth of the natural period of the accelerometer.[2]

The sensing element in a Statham accelerometer consists of an unbonded four-element, strain-sensitive, resistance-wire network, which may be represented electrically by a Wheatstone bridge. The accelerometer is calibrated by connecting a resistor across one arm of the transducer bridge. A deflection in the output circuit results

which corresponds to the effect of the combined resistance changes in the bridge arms due to a change in acceleration.[2]

Oscilloscopes. Through flexible cables, the output of the accelerometers are fed to two precalibrated Tektronix Type 535A oscilloscopes, one for each accelerometer.

The oscilloscopes transform the electrical pulses of each accelerometer into electrical waveform images which are called acceleration-time traces. These traces are photographed as they move across the calibrated screen by a Polaroid camera attached to each oscilloscope.

The vertical squares of the acceleration-time traces, (hereinafter referred to in this report as a-t traces), as scaled by the vertical distance between calibration pips, represent the gravity, or g, level produced by the acceleration-deceleration pulse, while the horizontal squares represent the time of acceleration, in milliseconds.

Some typical records are shown in Fig. 6.

## Data Reduction

Telereader and X-Y recorder. The first step in the data reduction process is to get the a-t traces onto graph paper. This is accomplished by placing the Polaroid prints of the a-t traces from the accelerometers on a Telecomputing Corporation Telereader and replotting to a larger scale.

Pace analog computer. A plot of the crushing mass a-t trace and a plot of the relative acceleration-time curve are traced over with

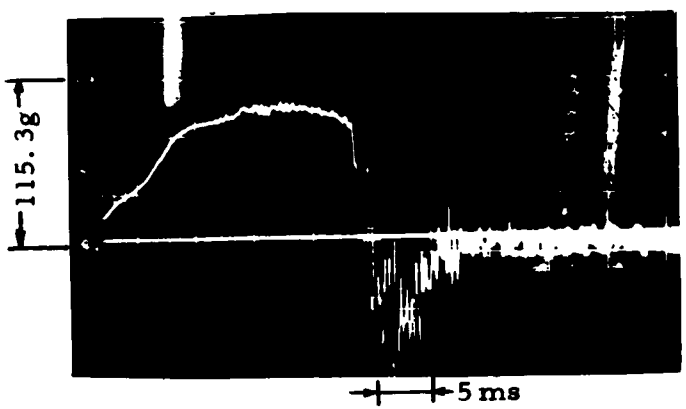


a. Carriage Acceleration for Vermiculite Concrete for Shot #53.

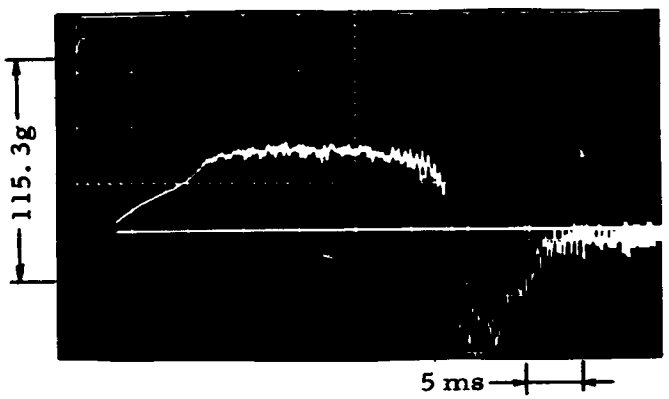


c. Carriage Acceleration for Foamed Plastic for Shot #52.

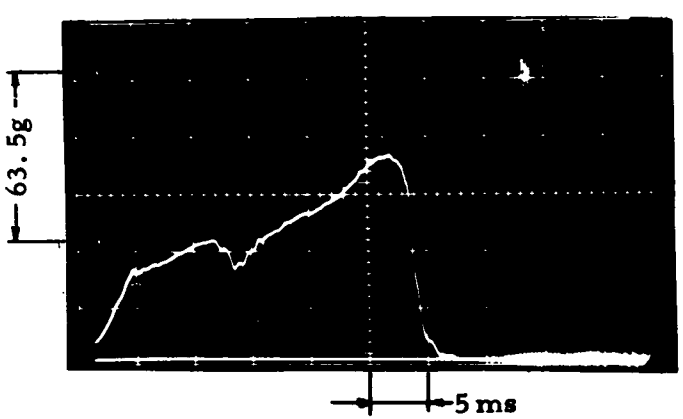


b. Crushing Mass Acceleration for Vermiculite Concrete for Shot #53.

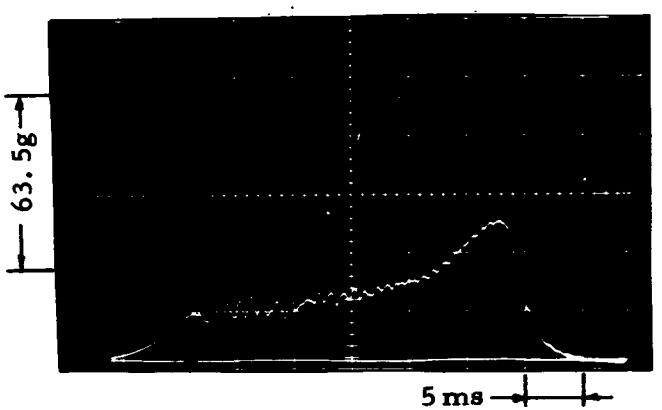


d. Crushing Mass Acceleration for Foamed Plastic for Shot #52.

Fig. 6. Typical Acceleration-Time Records for HYGE.

conducting ink. These are then fed into a Pace analog computer by using a curve follower. These curves were mathematically manipulated automatically by the computer and the output was in the form of stress-time and strain-time curves. These curves were then manually combined to obtain the stress-strain curve of the cushioning material tested. A complete description of this method is given in Appendix A. It should be mentioned that, by a more judicious electronic arrangement of the output signals of the accelerometers, manual plotting would have been reduced considerably.

CDC 1604 digital computer. An alternate method was developed mainly for future use and to serve as a check on the results obtained from the analog computer. Points on the graph of the a-t traces were used as input data for a FORTRAN program written for the Control Data Corporation 1604 digital computer available at the Computing Center, The University of Texas. The output of the digital computer was in the form of points of stress and strain. These points were then manually plotted to obtain the stress-strain curve of the cushioning material tested. A complete description of this alternate method is given in Appendix B.

It should be mentioned that, by using an X-Y plotter connected to a satellite computer that is now available for use with the CDC 1604, the stress-strain curve can be plotted automatically.

## Comparison of Analog and Digital Computer Results

Using the acceleration-time records from the same test firing,

stress-strain data was obtained by each of the two computer methods. A comparison of the results obtained from the two computer methods is shown in Fig. 7.

It is evident from Fig. 7 that the results are in close agreement. For the given test firing, the digital computer method gives approximately 1 per cent larger strain, approximately $\pm$ 4 per cent of the stress values, and approximately the same energy-absorption value when compared with the analog-computer method. This indicates that both methods of data reduction are valid. In general, all test firings that were compared had the same relative agreement of results.

It should be mentioned that, of the two computer methods used, there seems to be a greater probability for human error occurring when the analog-computer method is used to reduce data obtained from the HYGE. This is due mainly to the many steps in plotting and replotting intermediate curves before finally obtaining the stress-strain curve.

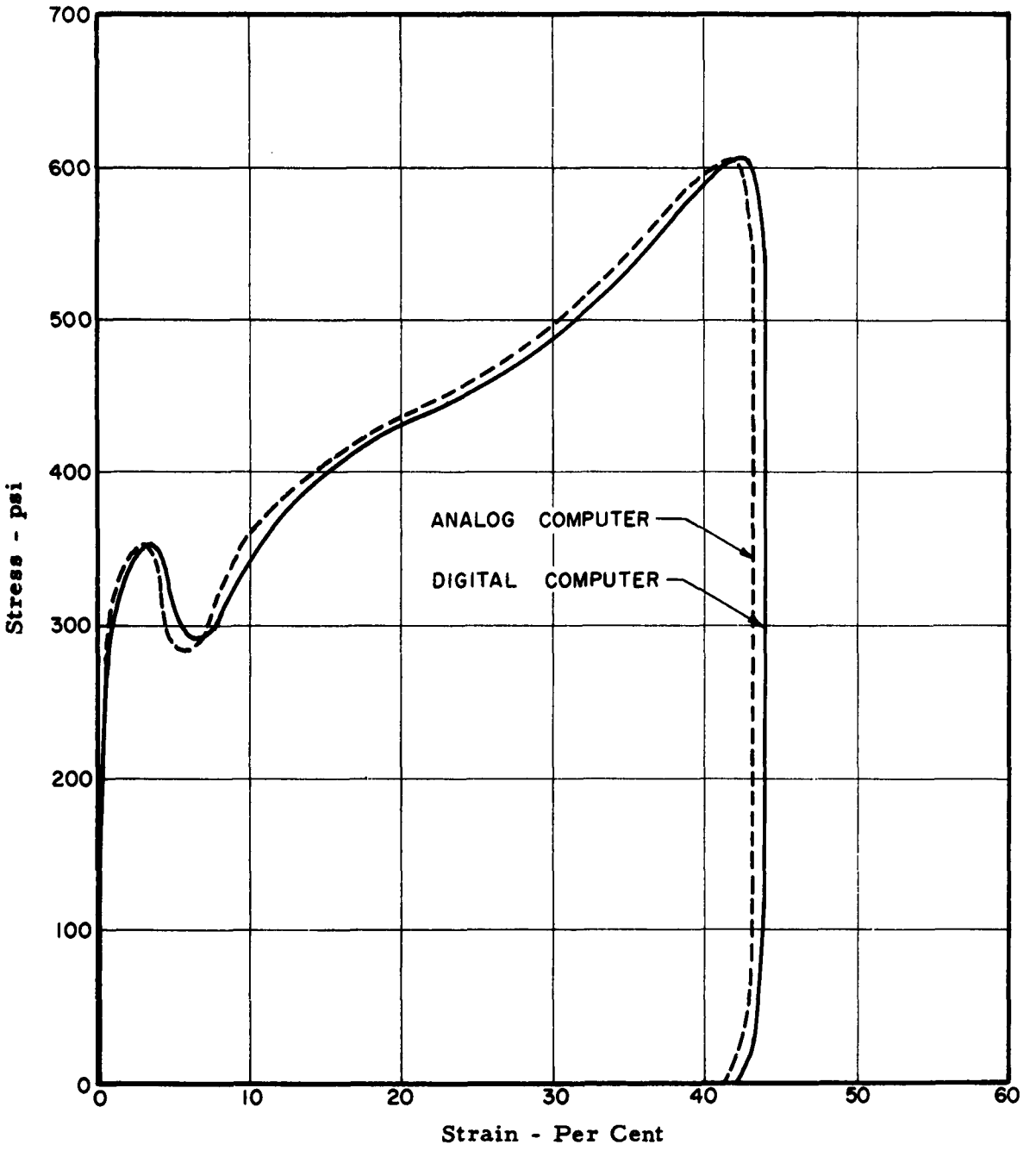


Fig. 7. Comparison of Analog and Digital Computer Results for Vermiculite Concrete.

## EXPERIMENTAL RESULTS

### Stress-Strain Curves for Vermiculite Concrete

Stress-strain curves for vermiculite concrete are presented in Fig. 8 for the complete range of carriage accelerations used in this investigation. Each stress-strain curve represents the average of two such curves made under approximately the same input conditions. A stress-strain curve for each individual firing for vermiculite concrete is given in Appendix C, Figs. C-1 through C-4.

The curves in Fig. 8 show that, to about 35 per cent strain, the stress value at a given strain value for each of the carriage accelerations is approximately the same; beyond 35 per cent strain, "bottoming"* begins to occur and seems to cause the curves to deviate from each other. Since the strain at which "bottoming" usually begins in vermiculite concrete is about 35 per cent, [1, 2] this strain value was chosen for this study to determine the energy dissipated. To make a comparison with the results from the drop tower, energy dissipated to 30 per cent strain was also determined. These values, as well as the total energy dissipated and average stress values to 35 per cent strain for vermiculite concrete, are given in Table 1.

The energy dissipated to 30 per cent strain was between 7.6 and 10.6 ft-lb per cu in., with an average value of 8.8 ft-lb per cu inch.

---

*Bottoming begins when all cavities in the material have collapsed. When this occurs, the slope of the stress-strain curve rises sharply. It begins shortly before maximum strain.

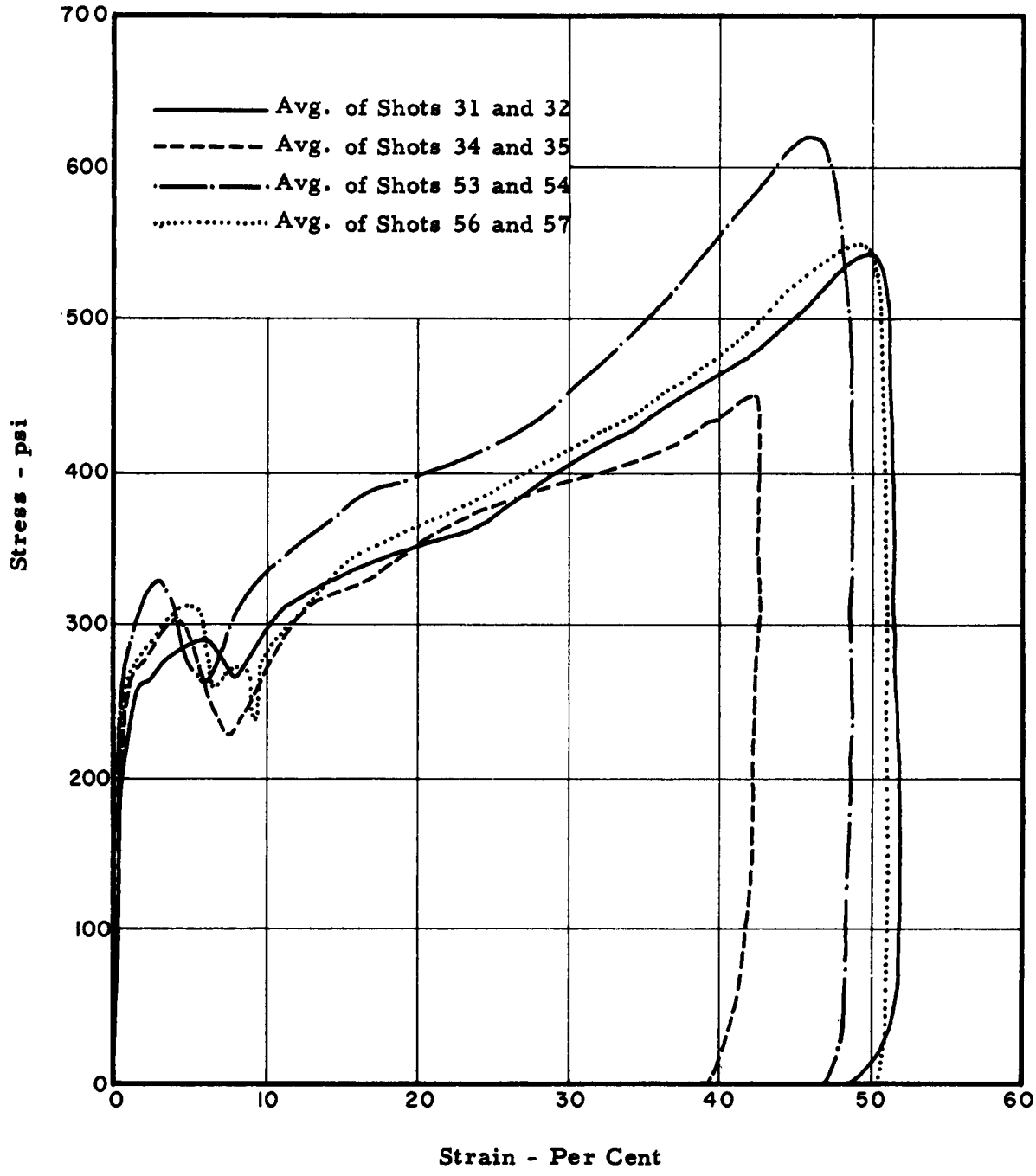


Fig. 8. Summary of Stress-Strain Curves for Vermiculite Concrete.

These values are in close agreement with the values previously determined using the drop tower[1] and the air gun.[2] Further, the average stress values to 35 per cent strain are between 300 and 400 psi. These values are in close agreement with those previously determined using the drop tower and air gun.[1, 2]

TABLE I

SUMMARY OF DATA FOR VERMICULITE CONCRETE

| Shot No. | Energy Dissipated to 30% Strain | Energy Dissipated to 35% Strain | Average Stress to 35% Strain | Approx. Max. Carriage Acceleration | Weight of Crushing Mass | Total Energy Dissipated |
|---|---|---|---|---|---|---|
| | ft-lb/in$^3$ | ft-lb/in$^3$ | psi | g | lb | ft-lb/in$^3$ |
| 31 | 7.6 | 9.2 | 300 | 119 | 70.6 | 17.7 |
| 32 | 8.9 | 10.8 | 350 | 125 | 70.6 | 16.1 |
| 34 | 8.6 | 10.2 | 330 | 105 | 70.6 | 11.9 |
| 35 | 7.9 | 9.5 | 300 | 105 | 70.6 | 12.6 |
| 53 | 10.6 | 12.9 | 400 | 87 | 98.5 | 16.1 |
| 54 | 8.5 | 10.2 | 340 | 89 | 98.5 | 19.2 |
| 56 | 9.3 | 10.3 | 345 | 65 | 126.7 | 15.9 |
| 57 | 8.7 | 10.4 | 350 | 61 | 126.7 | 18.8 |

## Stress-Strain Curves for Foamed Plastic

Stress-strain curves for foamed plastic are presented in Fig. 9 for the complete range of input accelerations used. Each stress-strain curve represents the average of two such curves made under approximately the same input conditions. A stress-strain curve for each individual firing for foamed plastic is given in Appendix C, Fig. C-5 through C-9.

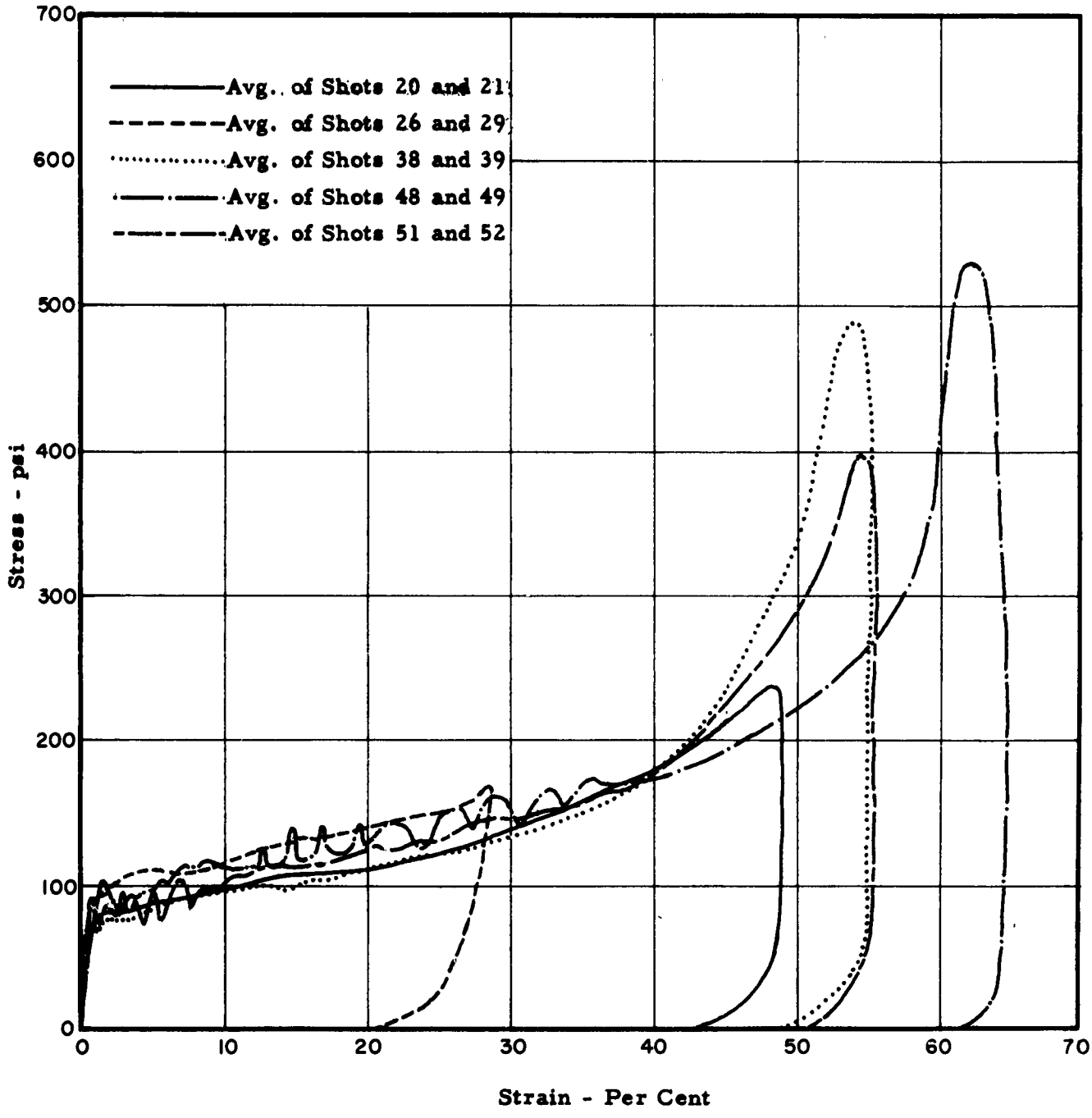


Fig. 9. Summary of Stress-Strain Curves for Foamed Plastic.

The curves in Fig. 9 show that, to about 40 per cent strain, the stress value at a given strain value for each of the carriage accelerations (with the exception of 100g input acceleration curve) is approximately the same. Since "bottoming" begins to occur at approximately 40 per cent strain, this strain value was chosen to determine the energy dissipated. Values for the energy dissipated to 40 per cent strain and total energy dissipated are given in Table II.

TABLE II

SUMMARY OF DATA FOR FOAMED PLASTIC

| Shot No. | Energy Dissipated to 40% Strain | Average Stress to 40% Strain | Approx. Max. Carriage Acceleration | Weight of Crushing Mass | Total Energy Dissipated |
|---|---|---|---|---|---|
| | ft-lb/in$^3$ | psi | g | lb | ft-lb/in$^3$ |
| 20 | 4.0 | 120 | 114 | 49.5 | 5.5 |
| 21 | 3.9 | 115 | 113 | 49.5 | 5.3 |
| 26 | * | * | 99 | 49.5 | 2.8 |
| 29 | * | * | 102 | 49.5 | 2.9 |
| 38 | 3.8 | 120 | 89 | 72.0 | 6.9 |
| 39 | 3.9 | 115 | 92 | 72.0 | 8.1 |
| 48 | 5.0 | 145 | 63 | 126.0 | 9.6 |
| 49 | 3.7 | 115 | 64 | 126.0 | 11.3 |
| 51 | 3.8 | 115 | 45 | 154.2 | 8.3 |
| 52 | 5.7 | 130 | 42 | 154.2 | 8.9 |

*Material did not exceed 30 per cent strain.

For the range of carriage accelerations used in this investigation, the energy dissipated to 40 per cent strain was between 3.7 and 5.7 ft-lb per cu in., with an average of 4.2 ft-lb per cu inch. This

average value is higher than the previously reported value of 2.9 ft-lb per cu in. obtained by using the drop tower.[3] Further, the average stress values to 40 per cent strain were between 115 and 145 psi, with an average of 122 psi. This average stress value is also slightly higher than the previously determined average stress of 110 psi.[3]

Configuration of Acceleration-Time Input Pulses

Acceleration-time input pulses for the HYGE, drop tower, and air gun are presented in Fig. 10. In this section, a brief description of how these input pulses were obtained will be given.

HYGE. The type of acceleration-time input pulse used in this investigation is shown by the solid line in Fig. 10. The input pulse was measured directly by an accelerometer mounted to the carriage, which is initially at rest, and is the pulse imparted to it by the thrust column assembly. It may be considered as a modified square pulse. The negative part of the a-t trace for the HYGE shown in Fig. 10 is the deceleration of the carriage after the input pulse is completed.

A diagram of the impact apparatus for the HYGE is shown in Fig. A-1 of Appendix A.

Drop tower. To obtain an acceleration-time input pulse for the drop tower, a stress-strain curve which had a maximum strain approximately that produced by using the HYGE was chosen from Ref. 1. This drop had an impact velocity of 10.8 fps. The a-t input pulse was obtained from the corresponding stress-time curve by using the following equation:

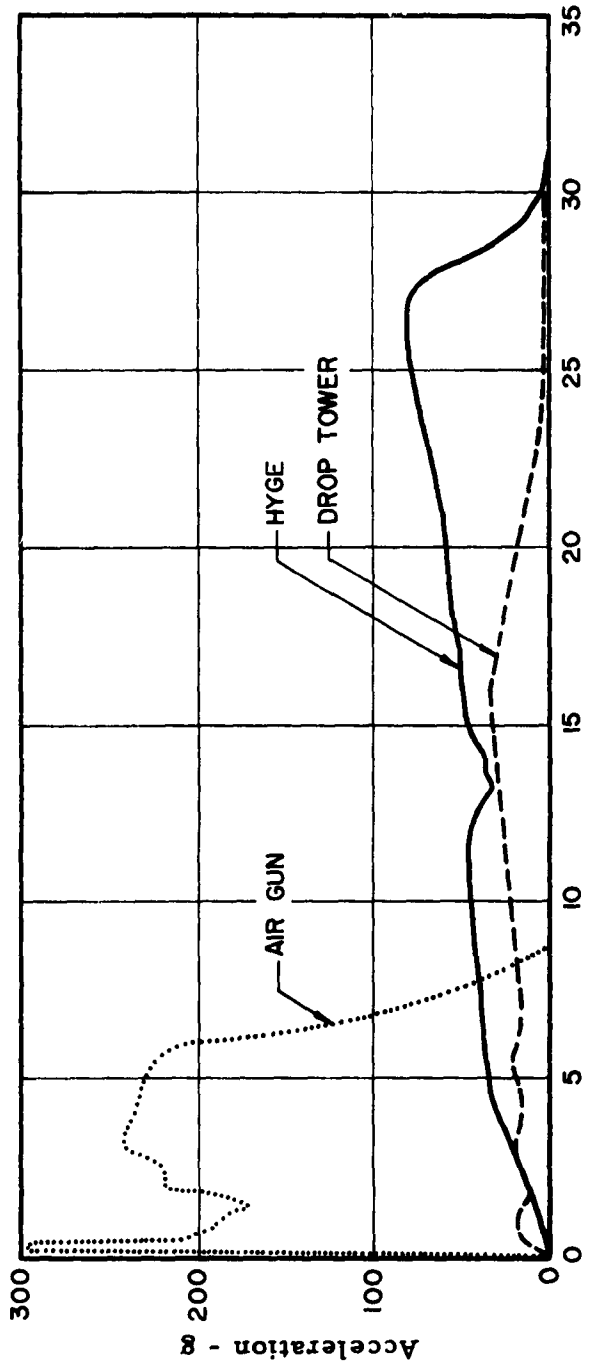


Fig. 10. Comparison of Acceleration-Time Input Pulse Shapes from Hyge Shock Tester, Air-Gun, and Drop-Tower

$$S(t) = \frac{F(t)}{A}$$

$$a_m(t) = \frac{S(t) \cdot A}{M_m}$$

where

$A$ = Impact area of the cushioning material.

$a_m$ = Acceleration of the impact mass.

$F(t)$ = Force on cushioning material as a function of time.

$M_m$ = Mass of the impact mass.

$S(t)$ = Stress on the cushioning material as a function of time.

The acceleration-time input pulse of the drop tower is thus determined indirectly, and is the pulse imparted to the cushioning material by the impact mass during impact. It is shown by the dashed line in Fig. 10 and may be considered as rectangular. Actually, however, the drop tower acceleration-time input pulse is a deceleration of the impact mass.

A photograph of the impact apparatus for the drop-tower facility is given in Fig. 1 of Ref. 3.

Air gun. To obtain an acceleration-time input pulse for the air gun, a stress-strain curve which had a maximum strain approximately equal to that produced by using the HYGE was chosen from Ref. 2. The impact velocity of the projectile for this shot was 60 fps. The a-t input pulse was obtained from the corresponding acceleration-time curve by using the following equation:[2]

$$a_p(t) = \frac{M_m}{M_p} \cdot a_m(t)$$

where

$a_m(t)$ = Acceleration of the particle as a function of time.

$a_p(t)$ = Acceleration of the projectile as a function of time.

$M_m$ = Mass of the cushioned mass.

$M_p$ = Mass of the projectile.

The acceleration-time input pulse of the air gun is thus also determined indirectly, and is the pulse imparted to the cushioning material by the projectile. It is shown by the dotted line in Fig. 10 and may be considered as rectangular. Like the pulse of the drop tower, it is a deceleration.

A diagram of the impact apparatus for the air gun is given in Fig. A-1 of Ref. 2.

Comparison of Acceleration-Time Input Pulses

From the acceleration-time input pulses shown in Fig. 10, the following comparisons may be observed:

1. The duration of the pulses of the drop tower and HYGE are about the same.

2. The duration of the pulse of the air gun is much less than the duration of the pulses of either the drop tower or HYGE.

3. The drop tower imparts accelerations to the cushioning material of lower magnitude than those imparted by the HYGE.

4. The air gun imparts accelerations to the cushioning material of much greater magnitude than those imparted by the drop tower or HYGE.

5. The rise time of the input pulse of the HYGE is much

longer than the rise time of the input pulses of the air gun and drop tower.

Comparison of Stress-Strain Curves for Vermiculite Concrete

Stress-strain curves for vermiculite concrete corresponding to the different acceleration-time input pulses are presented in Fig. 11. A sketch of the a-t input pulses is also shown in Fig. 11 for easy reference.

Similarities of stress-strain curves. In Fig. 11, it is evident that as the strain increases, the stress-strain curves exhibit a gradual increase in stress. This gradual increase continues until "bottoming" begins. After this occurs, the stress and strain are dependent on the severity of "bottoming." Also, if some of the oscillations are smoothed out, the average stress of each of the three dynamic stress-strain curves, to 30 per cent strain, is approximately the same. These similarities seem to occur despite the differences in the acceleration-time input pulses shown in the sketch in Fig. 11.

Differences of stress-strain curves. The following differences can be noted in the stress-strain curves shown in Fig. 11. These differences in the stress-strain curves will be explained in a later section.

1. To 30 per cent strain, the configuration of the stress-strain curve obtained from the HYGE more closely approximates the static stress-strain curve than either of the other two dynamic methods.

2. The stress-strain curve obtained from the HYGE has

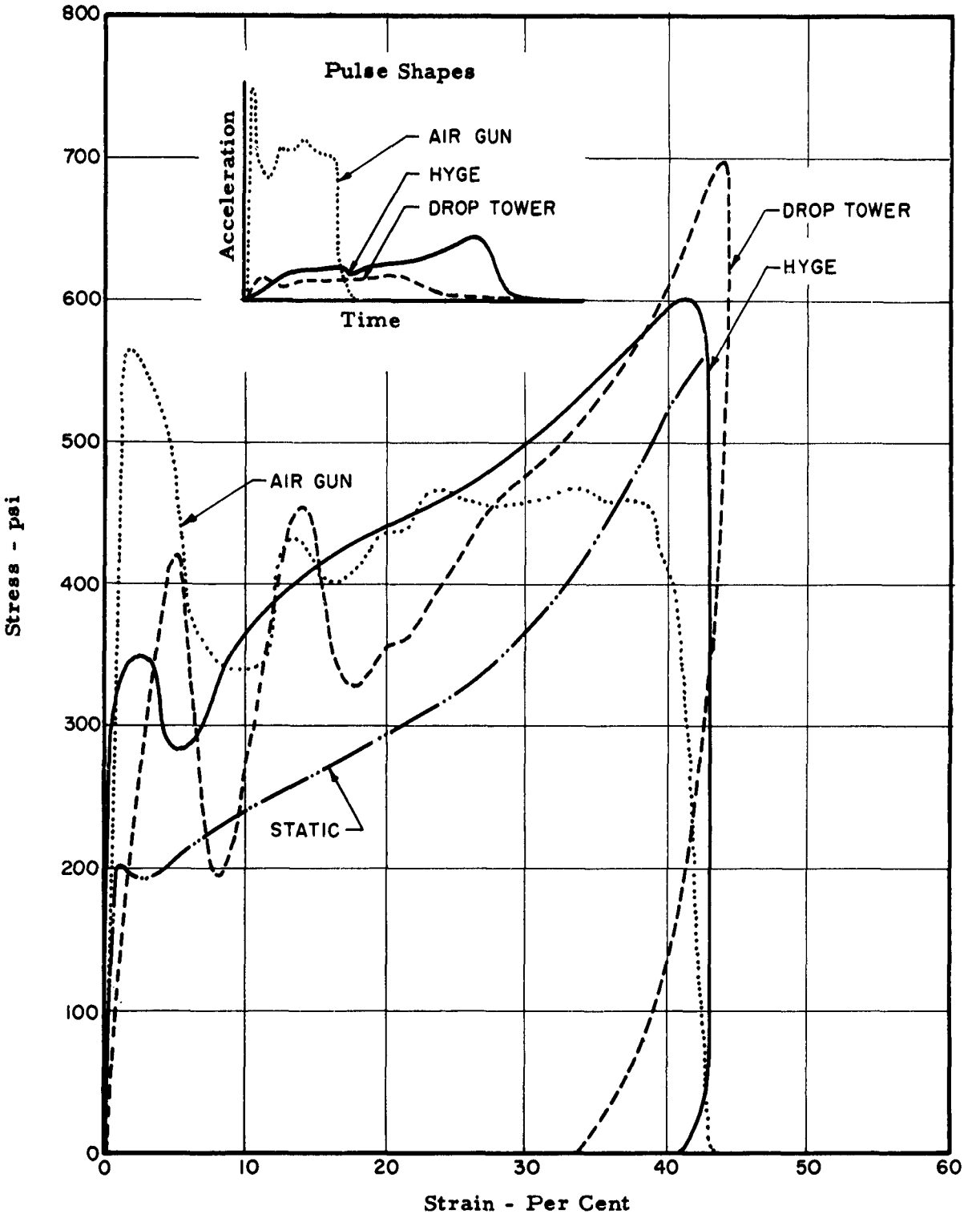


Fig. 11. Comparison of Stress-Strain Curves for Vermiculite Concrete from Hyge, Air-Gun, Drop-Tower and Statical Facilities.

fewer oscillations than the curves obtained by the other two methods.

3. More rebound results from using the drop tower than from using either of the other two methods.

4. The initial rise of the stress-strain curve from the HYGE has a greater slope than the initial rise of the stress-strain curves obtained from the drop tower, air gun, and static tests.

5. The initial peak of the stress-strain curve from the air gun is considerably higher than the initial peaks of the curves from the other two methods.

6. Oscillations from the drop tower are of longer duration than from the air gun or HYGE. This is not as evident in Fig. 11 as it is in the stress-strain curves in Ref. 1.

Explanation of Differences of Stress-Strain Curves

In Figs. 33 and 34 of Ref. 1, it was shown that the impact mass weight was not a factor in the shape of the stress-strain curve. In that study, the impact mass weight was a major variable. Although this effect was not considered in this study, nevertheless it is believed that the uniqueness of the shape of the stress-strain curve is a property of the material and not the results of the impact mass weight of the test method used. Hence, the following discussion will be limited to the differences in the stress-strain curves as a result of the use of different test methods. The following is an attempt to explain the differences in the stress-strain curves shown in Fig. 11.

Differences in test methods. It should be noted that there are some differences in the three dynamic test methods. First of all, the acceleration-time input pulses of the three methods are different. The configuration of the a-t input pulse is different in all three methods. The input pulse of the HYGE is medium in magnitude, and long in duration. The input pulse for the air gun is large in magnitude and short in duration, while that of the drop tower is low in magnitude and has a long duration. Also, for the HYGE, the a-t input pulse is an acceleration, while in the other two methods, it is actually a deceleration. The impact velocity for the air-gun test was 60 fps, while the impact velocity for the drop tower was only 10.8 fps. The HYGE tests start from rest.

In the HYGE and air-gun tests, the diameter of the impact area was 4 in., whereas in the drop tower, the diameter of the impact area was 6 inches. Thus, the impact areas for the HYGE and air-gun tests were 12.56 sq in., whereas the impact area for the drop tower was 28.3 sq inches.

Also, the projectile used as the impact mass for the HYGE and air-gun tests created a punching shear and bearing-type failure. The shearing resistance is included in the stress-strain curves which are presented in this report. The shear strength of vermiculite concrete is quite low in comparison with the compressive strength. Therefore, the effect of the shearing action on the stress-strain curves is believed to be very slight. In the drop tower, the shearing action was eliminated by using a plunger with the same diameter as the specimen. However, the results from the drop tower may have been affected somewhat by frictional resistance between the specimen and the confining cylinder.

If so, the effect on the stress-strain curve is essentially the same as the effect of the shearing action referred to above for the HYGE and air-gun tests. After the maximum strain has been reached in the HYGE and air-gun tests, the material tends to bind the plunger in such a way as to prevent some of the rebound from taking place. This type of frictional resistance was not present in the drop-tower test, since the plunger had the same diameter as the specimen.

These various differences in test methods undoubtedly create differences in the configuration of the stress-strain curves shown in Fig. 11.

Effect of type of force-sensing device. It is believed that the type of force-sensing device undoubtedly is a factor in the observance of oscillations in the stress-strain curves.

In general, it can be expected that more oscillations will be observed in the stress-strain curves from the drop tower than from the HYGE or air gun. This is due to an undamped, spring-mass, force-sensing device composed of a built-up force plate and dynamometer assembly used in the drop tower, whereas the other two methods used an accelerometer, which is a damped, spring-mass, force-sensing device. Thus, the amplitudes of the natural frequencies of oscillations of the force-plate assembly will damp out slowly and will continue for a relatively long period of time. On the other hand, since the value of the damping factor of the accelerometer is very near the critical value, the vibrations of its mass are quickly damped out. This effect is exhibited in the resulting stress-strain curves.

Combined effect of rate of loading and the type of force-sensing device. It is also believed that the rate of application of the impact force and the type of force-sensing device has an effect on the number of oscillations observed and the amplitude of the initial peak exhibited in the stress-strain curves.

The rate of application of the impact force influences the overshoot of the force-sensing device. The overshoot, in turn, influences the amplitude of the initial peak and amplitudes of succeeding oscillations of the stress-strain curve. If the rate of application is very rapid and an accelerometer is used, the accelerometer will considerably overshoot the initial portion of the acceleration-time input pulse. As a result, the first peak of the stress-strain curve may be quite large, and the amplitudes of succeeding oscillations may be relatively large, but they should damp out quickly. This is the case of the air gun. On the other hand, if the rate of application is slow and an accelerometer is used, it will follow the acceleration-time input pulse with very little overshoot. The small amount of overshoot will be quickly damped out and a relatively smooth stress-strain curve will result, as is the case of the HYGE.

In the case of the dynamometers, a very rapid application of impact force also causes a type of overshoot, but these oscillations are damped out slowly. Thus, the resulting stress-strain curve should exhibit several oscillations (generally, more than the air gun).

## Comparison of Stress-Strain Curves for Foamed Plastic

Stress-strain curves for foamed plastic corresponding to the

acceleration-time input pulses from the HYGE and drop tower are presented in Fig. 12. It should be mentioned that the curve shown for the drop tower is an average of several stress-strain curves. It is not the original curve for a particular stress-strain curve in Ref. 3. A sketch of the two a-t input pulses is also shown in Fig. 12 for easy reference. The explanations given previously are, in general, valid for the stress-strain curves for foamed plastic shown in Fig. 12. To the previous explanations for the differences in test methods should be added that the HYGE test was a totally confined test on a 6-in. -diameter by 6-in. -height specimen, whereas the drop tower test was an unconfined test on a 24 x 24 x 6-in. pad. It was believed, however, that the dimensions of the pad would render it as having nearly the same effect as a confined test.

The following comparisons refer only to the stress-strain curves shown in Fig. 12.

1. The amplitudes of the oscillations and the distance between peak to peak of the stress-strain curve from the drop-tower are considerably greater than those of the stress-strain curve from the HYGE.

2. The average stress to 40 per cent strain is higher for the HYGE curve than for the drop tower curve.

3. More rebound occurs by using the drop tower than by using the HYGE.

4. The initial portion of the stress-strain curve for the HYGE has a considerably greater slope than the same portion of the stress-strain curve for the drop tower.

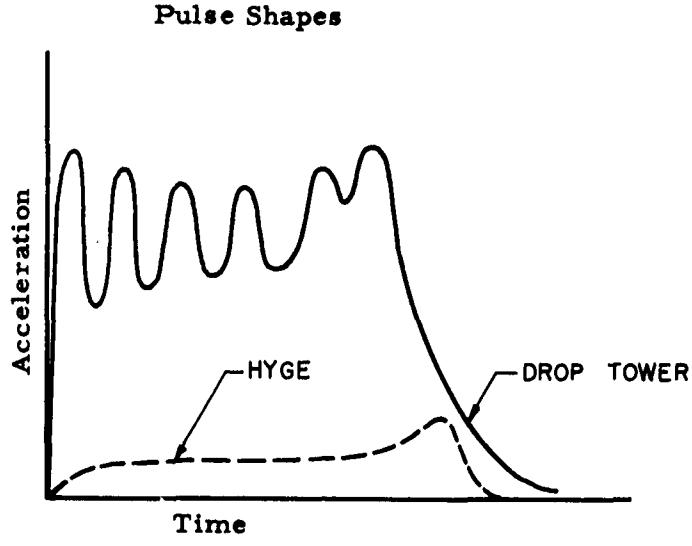


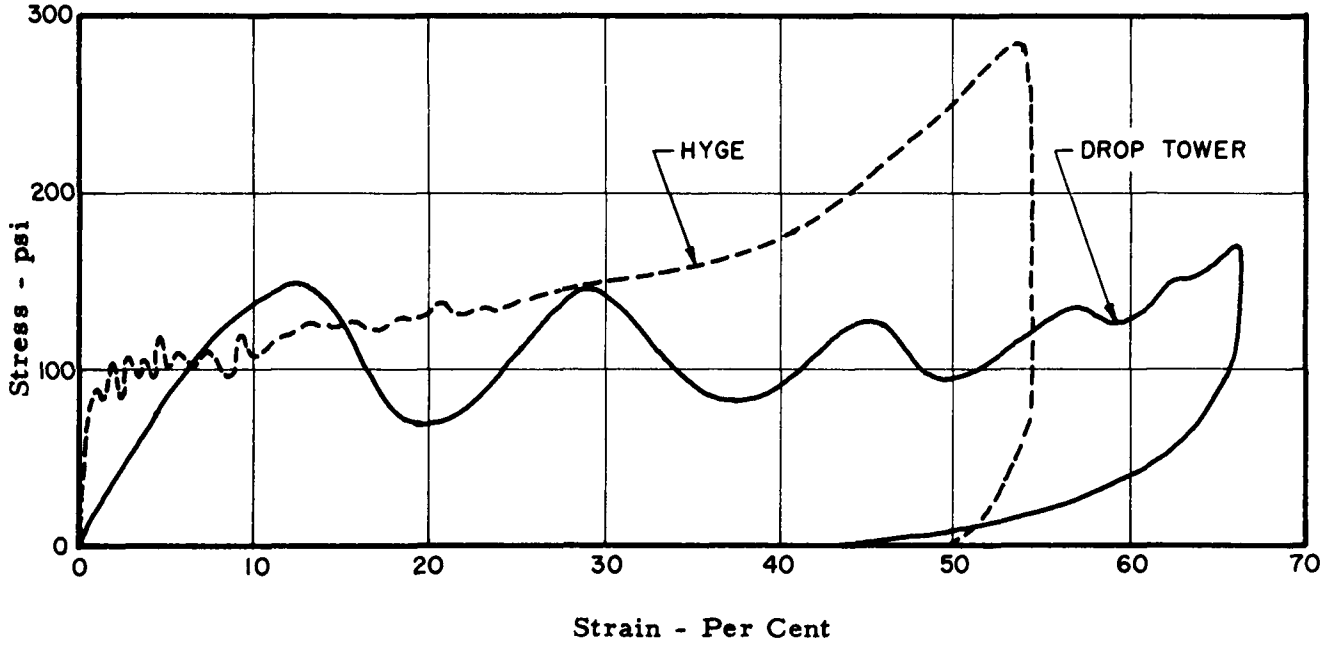


Fig. 12. Comparison of Stress-Strain Curves for Foamed Plastic from Drop Tower and HYGE.

5. "Bottoming" is more severe for the HYGE test than for that of the drop tower. (This is due to the test specimen being unconfined for the drop tower test).

## VALIDITY OF RESULTS

### Extrapolation of Acceleration-Time Records to Obtain Starting Point

From the typical acceleration-time traces from the HYGE shown in Fig. 6, it can be observed that the triggering device used did not permit picking up the beginning of the trace.

As previously stated, two computer methods were used in reducing the data for this report. Programs were developed independently for these methods by two of the authors. One acceleration-time record was reduced by each of the two programs. However, in reducing the data with the digital computer, a straight line from the beginning of the a-t traces was projected vertically down to the time axis. In using the analog computer, the a-t trace was projected back to the time axis with a slope equal to the slope of the initial portion of the a-t trace. This resulted in a difference in total strain of approximately 10 per cent. However, when the authors used the same starting point, a much closer comparison resulted as indicated in Fig. 7. This study emphasizes the importance of using a uniform procedure in establishing the starting point of the a-t trace.

All of the stress-strain curves presented in this report were obtained by using the starting point determined by projecting the a-t traces to the time axes on the same slopes as the initial portions of the a-t traces.

### Uniformity in Test Results

Each of the figures in Appendix C for the vermiculite concrete

and foamed plastic have stress-strain curves for two identical tests, i.e., the crushing mass and carriage acceleration were held constant for the two tests. The figures show the resulting variation in data from the two tests. Sources of variation include (1) projection of the acceleration curve back to the time axis to obtain a starting point, (2) small variations in density of the two specimens, (3) heterogeneity of the specimens (much more so for the foamed plastic than for the vermiculite concrete, and (4) small instrumentation errors.

## Reliability of Acceleration-Time Measurements

Calculations were made to compare the maximum strain obtained by double-integration of the a-t traces, with the permanent strain which was measured after crushing of the specimen had taken place. These calculations were made in order to verify the accuracy of the accelerometers and of the computer results. The maximum difference between the measured and calculated strain was less than 5 per cent.

Some crushing takes place during firing after the thrust has terminated and the acceleration of the carriage has been reduced to zero. Further crushing continues even during deceleration of the carriage. This condition is represented by the cross-hatched area in Fig. 13.

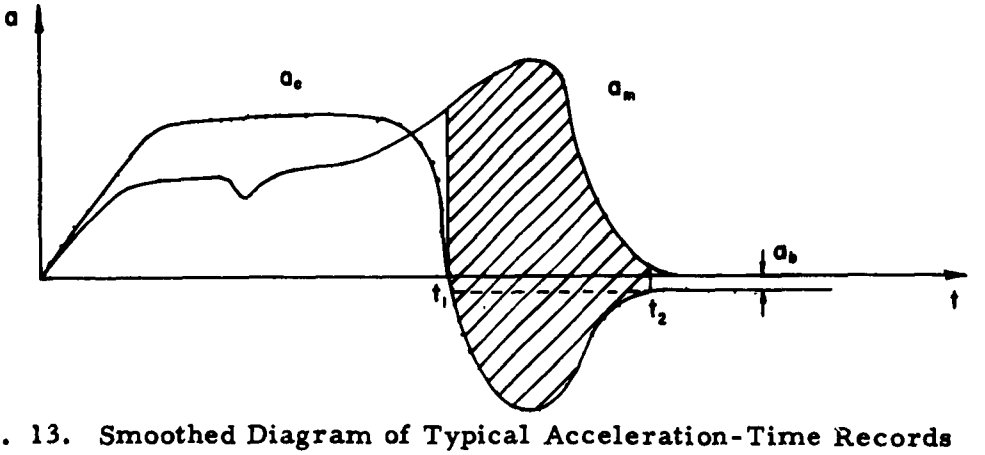


Fig. 13. Smoothed Diagram of Typical Acceleration-Time Records

During crushing, the force of the crushing mass on the specimen must be in equilibrium with the force of the specimen on the crushing mass. The specimen moves with the carriage during crushing. During the time interval corresponding to the cross-hatched portion in Fig. 13, the only external force acting on the carriage is a small deceleration force applied by the carriage brakes. The force of gravity acts on both the crushing mass and the carriage. It is neglected in this discussion. The following equations must be satisfied during the time interval corresponding to the cross-hatched area:

$$M_m \cdot a_m = M_c \cdot (a_c - a_b) \qquad \ldots\ldots (1)$$

where

$a_b$ = Deceleration due to carriage brakes.

$a_c$ = Acceleration of the carriage.

$a_m$ = Acceleration of the crushing mass.

$M_c$ = Mass of carriage assembly (including carriage, restraining frame, and specimen.)

$M_m$ = Mass of crushing mass.

or, over a finite time interval,

$$\int_{t_1}^{t_2} M_m \cdot a_m \cdot dt = \int_{t_1}^{t_2} M_c \cdot (a_c - a_b) \cdot dt \qquad \ldots\ldots (2)$$

where $t_1$ and $t_2$ are any two distinctly different points within the cross-hatched portion of Fig. 13.

Rearranging,

$$\frac{M_m}{M_c} \int_{t_1}^{t_2} a_m \cdot dt = \int_{t_1}^{t_2} (a_c - a_b) \cdot dt \qquad \ldots\ldots (3)$$

It should be mentioned that the deceleration $a_b$ occurs throughout the travel of the carriage and is believed to be nearly constant. The comparatively large magnitude of deceleration of the carriage as shown in Fig. 13 is caused for the most part by bottoming of the crushing mass. After crushing is complete, the crushing mass and the specimen can lose contact with the carriage. This is due to the carriage decelerating at a faster rate than the specimen and crushing mass, until the crushing mass strikes the top of the restraining frame.

Eq. (3) was used to make a check on several of the curves, and the equation was satisfied within $\pm 5$ per cent. This check signifies that the accelerometer measurements can be considered as reliable.

# CONCLUSIONS

## Vermiculite Concrete

The following conclusions apply to the input acceleration range of 61 to 125g, and to the crushing mass range of 70.6 to 126.7 pounds.

1. Vermiculite concrete of approximately 46 lb per-cu-ft-density dissipates approximately 10.4 ft-lb per cu in. of energy up to 35 per cent strain at a stress of approximately 340 lb per sq in. under modified square wave pulse produced by the HYGE.

2. The average stress and energy dissipation up to similar limiting strains, as well as total energy dissipation, are in agreement with the results obtained with the 275-ft drop tower and 4-in. bore air-gun facilities.

3. The stress-strain curve due to the input pulse of the HYGE closely approximates the configuration of the static stress-strain curve.

4. Results obtained from the HYGE more nearly approximate the results of the drop tower, considerably more so than the results from the air gun.

5. The dynamic stress obtained from the HYGE is approximately 1-1/2 times the static stress, to 30 per cent strain, for all levels of acceleration.

6. Stress-strain curves obtained from the HYGE did not have any significant oscillations. In contrast, the stress-strain curves from the drop tower and air gun had several.

7. If the oscillations of the stress-strain curves for vermiculite concrete obtained from the variable input pulses of the HYGE, the air-gun, and the drop tower are smoothed, the results from these three facilities are essentially in agreement to 35 per cent strain. Thus, the shape of the load pulse has little effect upon the shock-mitigating characteristics of vermiculite concrete.

Foamed Plastic

The following conclusions apply to an input acceleration range of 42 to 115g and to a crushing mass range of 49.5 to 154.2 pounds.

1. Quartermaster polyurethane-plastic 108C with a density of 6 lb per cu ft dissipates approximately 4.2 ft lb per cu in. of energy to 40 per cent strain at an average stress of 120 psi under a modified square wave produced by the HYGE.

2. The average stress and the energy dissipated to 40 per cent strain are slightly lower than those determined using the drop tower.

3. Stress-strain curves obtained from the HYGE have oscillations with amplitudes which are less than those obtained from the drop tower.

4. Less rebound results from the HYGE than the drop tower.

Computer Methods

1. The results from both the analog and digital computer methods were in very close agreement.

2. Both the analog and digital computer methods are valid for reducing the data to stress-strain curves.

3. The method used will depend on the computer facilities available, and is a matter of convenience and preference.

# RECOMMENDATIONS

## Constant Crushing Mass

The following recommendations are made with the stipulation that the weight of the crushing mass be kept constant:

1. The effect of variation of input acceleration on total energy absorption, peak stress, average crushing stress, and energy-absorption to "bottoming" should be investigated.

2. A stress-strain curve should be plotted for each input acceleration used. Each curve should be plotted as one of a family of stress-strain curves to visually indicate the effect of variation input acceleration on the stress-strain properties of the cushioning material.

3. The effect of variation of rate of strain on the energy-absorption properties of the cushioning material should be investigated.

## Constant Input Acceleration

The following recommendations are made with the stipulation that the input acceleration be kept constant:

1. The effect of variation of crushing mass on the energy-absorption value to "bottoming" should be investigated.

2. The effect of variation of crushing mass required to produce "bottoming" of a given surface area of cushioning material should be investigated.

## BIBLIOGRAPHY


1. Covington, C., Dynamic Energy-Absorbing Characteristics of Lightweight Vermiculite Concrete, DASA 1238, Austin, Structural Mechanics Research Laboratory, The University of Texas, 1961.

2. Shield, R., et al, Shock Mitigation with Lightweight Vermiculite Concrete, DASA 1263, Austin, Structural Mechanics Research Laboratory, The University of Texas, 1962.

3. Shield, R., and Covington, C., High-Velocity Impact Cushioning, Part VI, 108C and 100C Foamed Plastics, Austin, Structural Mechanics Research Laboratory, The University of Texas, September, 1960.

4. _____, Bulletin 4-70, Consolidated Vacuum Corporation, Rochester 3, New York.

5. Kunz, K. S., Numerical Analysis, McGraw-Hill Book Company, Inc., New York, 1957, p. 146.

# APPENDIX A

## APPENDIX A

## CONVERSION OF ACCELERATION-TIME CURVES TO STRESS-STRAIN CURVES USING AN ANALOG COMPUTER

### Notation

The following notation is adopted for use in this appendix only.

$a_b$ = Deceleration due to carriage brakes

$a_c$ = Acceleration of the carriage

$a_d$ = Relative acceleration of the carriage and crushing mass

$a_m$ = Acceleration of the crushing mass

$A$ = Impact area of the impact mass

$\delta_c$ = Displacement of the carriage

$\delta_m$ = Displacement of the crushing mass

$\delta_d$ = Relative displacement of the carriage and crushing mass

$\varepsilon$ = Unit Strain in the cushioning material

$F_m$ = Resisting force of the cushioning material, in pounds

$H_o$ = Initial height of the cushioning material

$H_{cr}$ = Crushed height of the cushioning material

$M_1$ = Nonvariable mass

$M_2$ = Variable mass

$M_c$ = Mass of carriage

$M_m$ = Crushing mass; $\Sigma(M_1 + M_2)$

$\sigma$ = Stress in the cushioning material

$t$ = Time after firing

## Schematic Representation of Impact Arrangement

A diagram of the impact arrangement which indicates the location of the accelerometers and other pertinent information is shown in Fig. A-1. This information is also shown in Fig. 5.

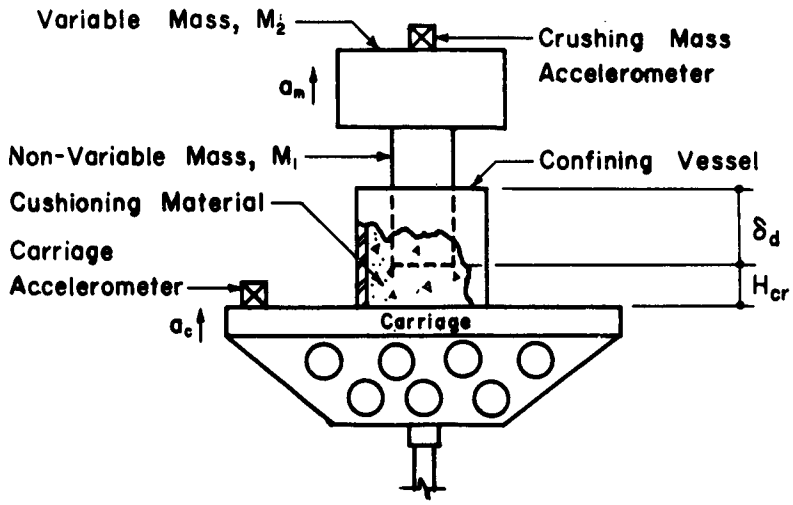


Figure A-1. Impact Apparatus Arrangement

## Description of Conversion Technique

The accelerations of the carriage and crushing mass during firing were recorded as a function of time by instrumentation previously described. The following procedure was used to obtain the stress-strain curve of the cushioning material.

A Telereader, used in conjunction with an X-Y recorder, was used to enlarge and replot the acceleration-time curves of both the

carriage and crushing mass on 11 x 16-1/2-in. graph paper. This was done for each firing. An example is shown in Fig. A-2. The relative acceleration was then manually plotted as a function of time by use of Eq. (A-1):

$$a_d(t) = a_c(t) - a_m(t) \qquad \text{- - - - - (A-1),}$$

where the relative acceleration $a_d$ represents the difference in acceleration between the carriage and the crushing mass. An example of this curve is shown in Fig. A-3. The relative acceleration curve was then traced over with conducting ink so that a curve follower could be used to read this acceleration-time data into an analog computer.

Strain-time curve. The analog computer performed the integration and summation processes as given in Eqs. (A-2) and (A-3) to obtain strain-time data.

$$\int_o^t \int_o^t a_d(t)dt \cdot dt = \delta_c(t) - \delta_m(t) = \delta_d(t) \qquad \text{- - - - - (A-2)}$$

$$\varepsilon(t) = \frac{\delta_d(t)}{H_o} \qquad \text{- - - - - (A-3)}$$

The strain-time data was then fed into an X-Y recorder and it automatically plotted a strain-time curve. A typical strain-time curve for vermiculite concrete is shown in Fig. A-4 as an illustration.

Stress-time curve. The stress in the cushioning material was

obtained as a function of time by having the analog computer apply the constants given in Eq. (A-4) to the acceleration-time data for the crushing mass.

$$F_m = M_m \cdot a_m(t)$$

$$\sigma(t) = \frac{F_m}{A} = \frac{M_m \cdot a_m(t)}{A} \qquad \text{- - - - - (A-4)}$$

This stress-time data was fed into an X-Y recorder and it automatically plotted a stress-time curve. A typical stress-time curve for vermiculite concrete is shown in Fig. A-4 as an illustration.

Functional diagram of analog-computer circuits. The analog-computer circuits used to make the above-mentioned computations are represented in the form of a functional diagram and are given in Fig. A-5. The necessary scale factors and pot (potentiometer) settings are also given in that figure.

Stress-strain curve. A stress-strain curve for each firing was manually plotted by taking points from the appropriate stress-time and strain-time curves at various values of time. This is illustrated in Fig. A-4. A typical stress-strain curve for vermiculite concrete is given in Fig. A-6 as an illustration of the results of this technique.

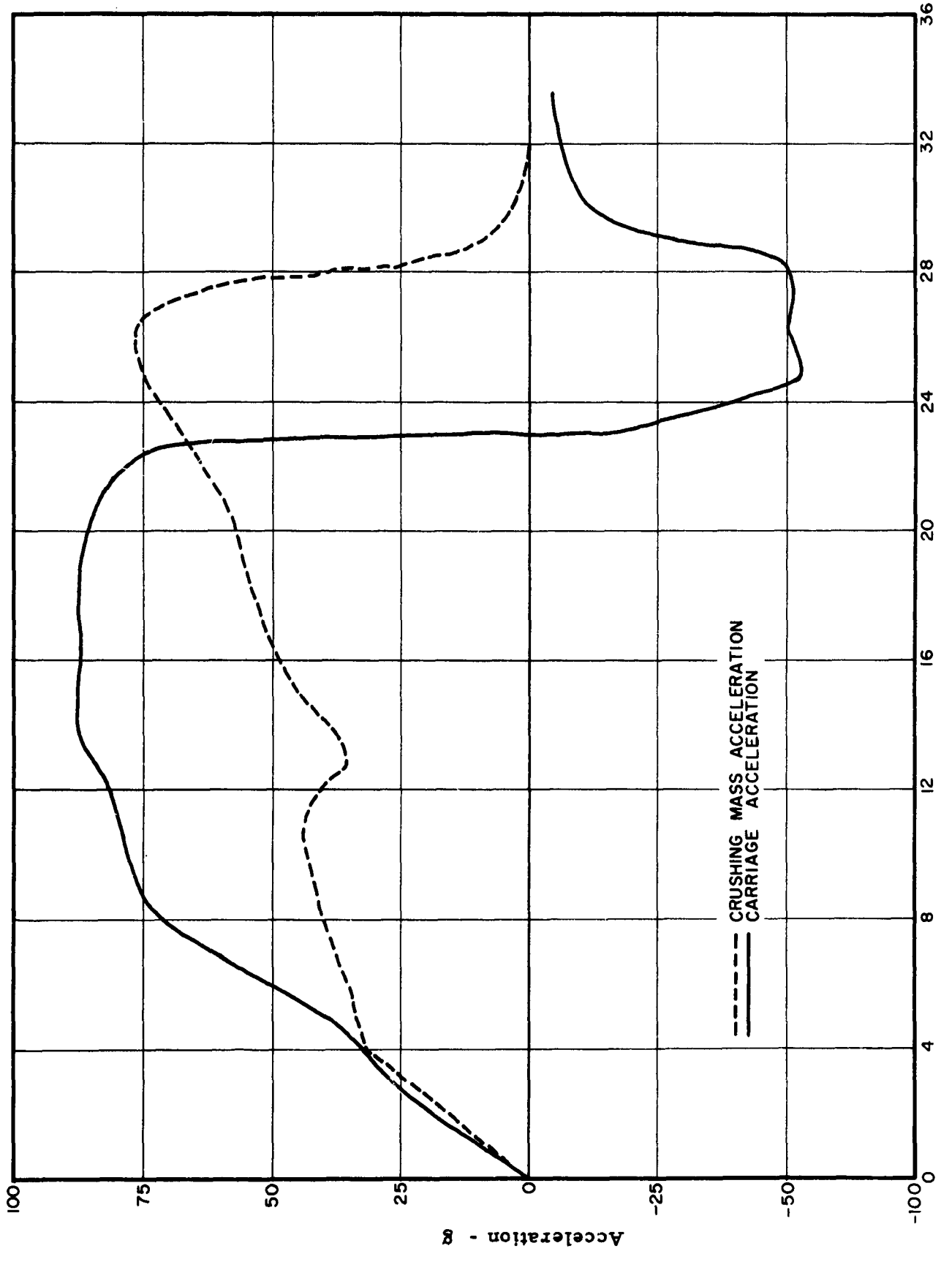


Fig. A-2. Example of Enlargement and Replotting of Acceleration-Time Curves from Photographs.

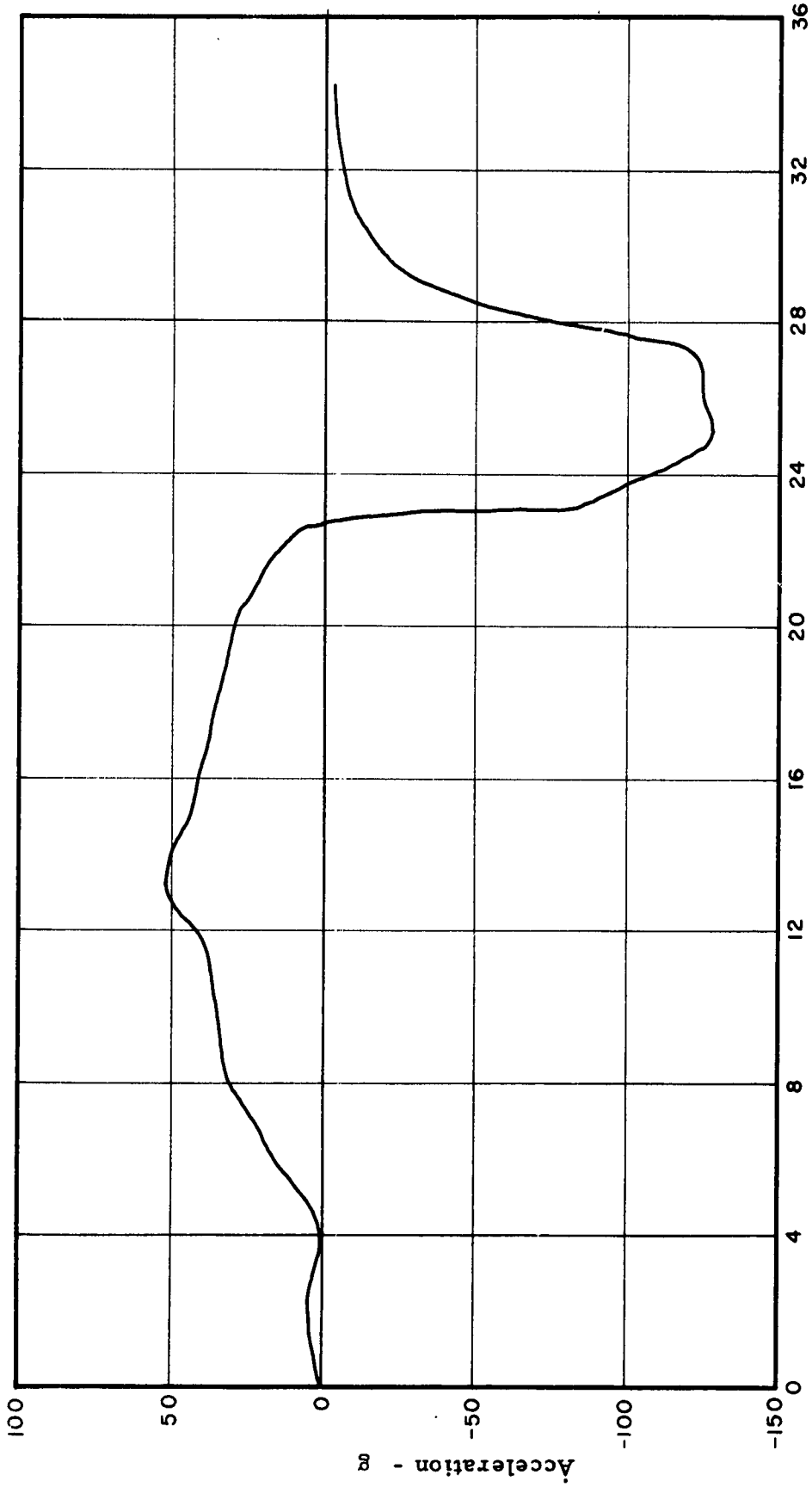


Fig. A-3. Example of the Difference between the Carriage and Crushing Mass Acceleration-Time Curves.

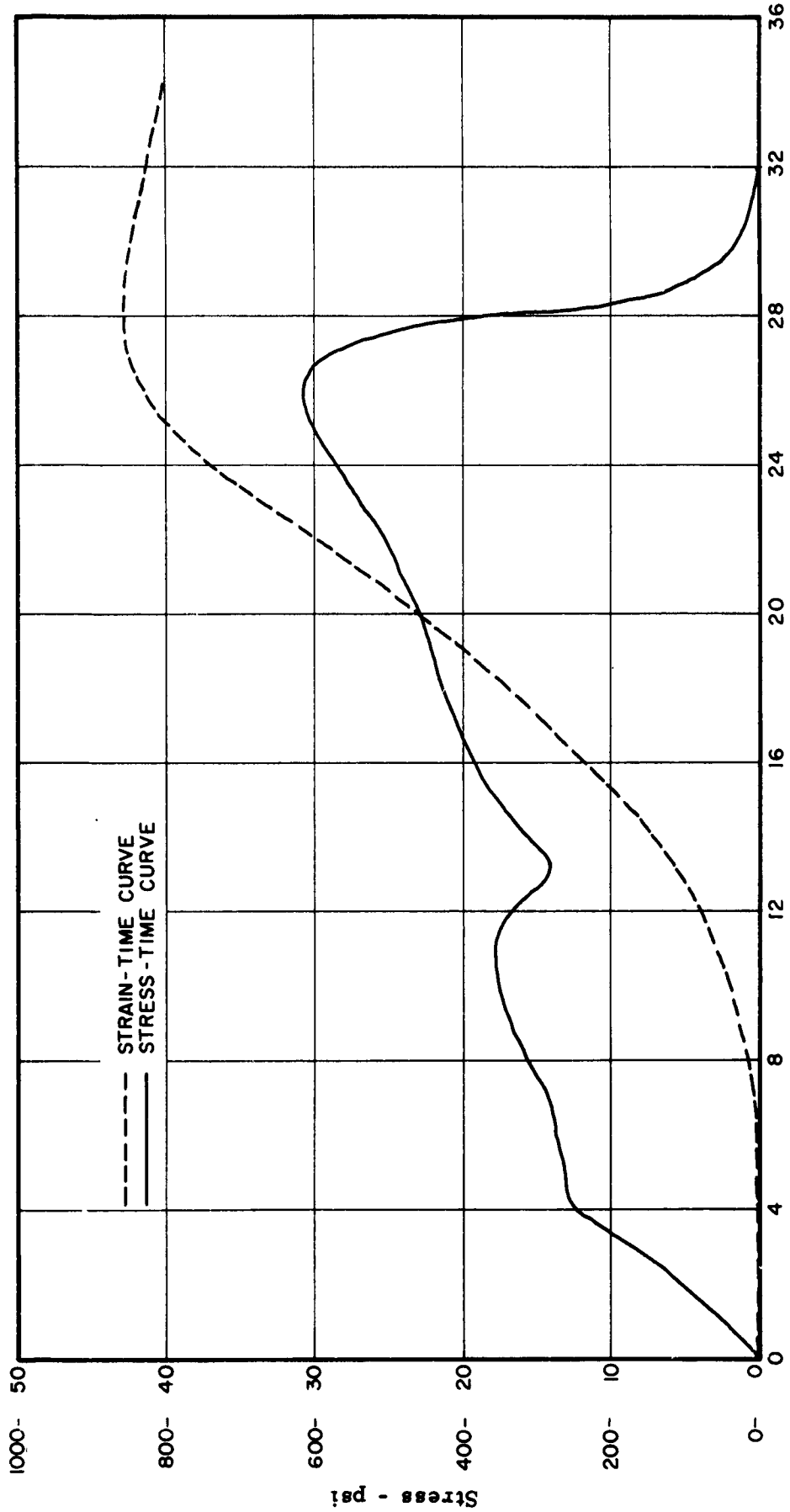


Fig. A-4. Typical Strain-Time and Stress-Time Curves for Vermiculite Concrete.

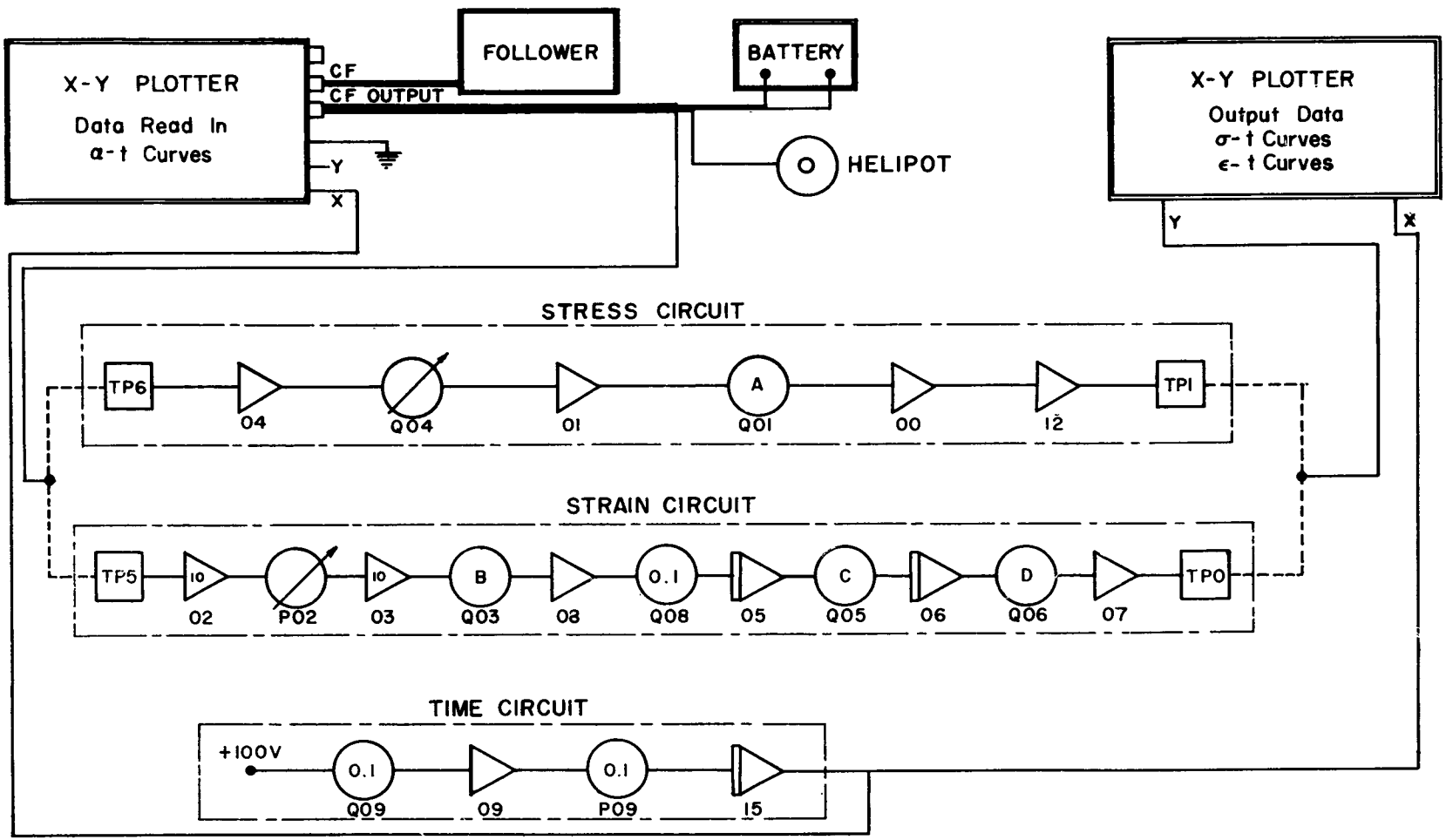


SCALE FACTORS

$B_t = \frac{0.045}{75} = 0.0006$

$A_{\ddot{x}} = 32.2 \frac{FT/SEC}{V}$

$A_{\dot{x}} = 2 \frac{FT/SEC}{V}$

$A_x = 250 \frac{FT}{SEC}$

POT SETTINGS

$A = \frac{M}{A} (10^{-1})$

$B = 10 (A_{\ddot{x}} B_t A_x) = 0.3864$

$C = \frac{A_x}{A_{\dot{x}}} B_t = 0.075$

$D = \left(\frac{1}{A_x}\right)\left(\frac{1}{L}\right)(10^2)$

**Fig. A-5. Functional Diagram of Analog Computer Circuits**

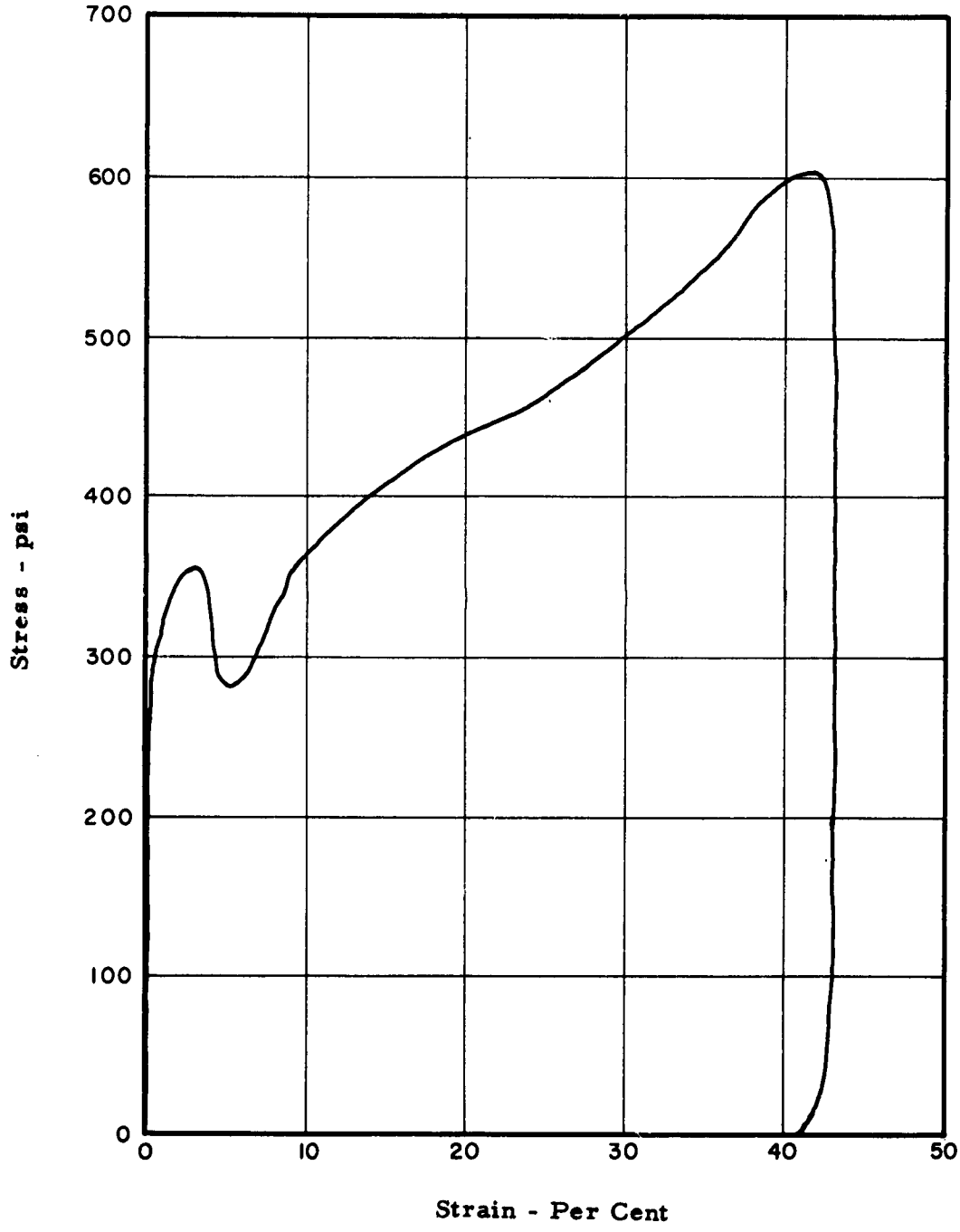


Fig. A-6. Typical Stress-Strain Curve for Vermiculite Concrete.

# APPENDIX B

## APPENDIX B

## CONVERSION OF ACCELERATION-TIME CURVES TO STRESS-STRAIN CURVES USING A DIGITAL COMPUTER

### Notation

The following notation, adopted for use with the digital computer only, was used in conjunction with the quadrature expression and the flow diagram given in this appendix:

| | | |
|---|---|---|
| A(i) | = | Relative acceleration, or [CA(i) - SA(i)] |
| B | = | Cross-sectional area of the crushing mass |
| CA(i) | = | Carriage acceleration, at any given time i |
| E(i) | = | Engineering strain, at any given time i |
| H | = | Time interval between readings |
| K | = | 0 or 1. (0 if more than one problem to be solved; 1 if only one) |
| LA | = | Indicator (for internal operation of the program) |
| M | = | Number of data values |
| S(i) | = | Engineering stress, at any given time i |
| SA(i) | = | Crushing mass acceleration, at any given time i |
| V(i) | = | Relative velocity, at any given time i |
| X(i) | = | Relative displacement, at any given time i |
| XL | = | Initial height of the cushioning material |
| XM | = | Crushing mass |

### Description of Conversion Technique

The accelerations of the carriage and crushing mass were recorded

photographically as a function of time. To convert the photographic data to stress-strain data of the cushioning material, the following procedure was used.

Each photograph was placed in a Universal Telereader and, by using two digital voltmeters and a scanner coupler, acceleration-time values at selected intervals were digitized and punched on photo-electric tape by an auxiliary punch. The punched paper tape was then fed into the digital computer as input data.

The computer then digests all the data, translating it into machine language to permit manipulation of the numbers, and performs double integration numerically through the use of a quadrature expression. Thus, from the initial acceleration-time functions, and by using appropriate mathematical formulations, stress-time and strain-time functions are automatically obtained. These two functions are then automatically combined by the computer to form the stress-strain values.

The output, which is printed on paper, lists the carriage acceleration values, crushing mass acceleration values, and the resulting stress and corresponding strain values for each test firing.

## Mathematical Formulations

The symmetric quadrature formula[5]

$$\int_{x_0}^{x_1} f(x) \cdot dx = (h/3) \left[(f_o + 4f_1 + f_2)\right]$$

known as Simpson's One-Third Rule, was used in two forms in this

appendix to double integrate the acceleration-time curve to obtain the displacement-time data.

The following formulas were used to obtain the stress-strain data:

$$A(i) = CA(i) - SA(i) \qquad \text{- - - - - (1)}$$

$$V(i) = (H/3) \cdot [A(i-2) + 4A(i-1) + A(i)] \qquad \text{- - - - - (2)}$$

$$X(i) = (H/3) \cdot [V(i-2) + 4V(i-2) + V(i)] \qquad \text{- - - - - (3)}$$

$$E(i) = X(i)/XL \qquad \text{- - - - - (4)}$$

$$S(i) = [SA(i)] \cdot [XM]/B \qquad \text{- - - - - (5)}$$

Flow Diagram

The flow diagram, which utilizes the above mathematical formulations in the processing of the program through the computer, is shown in Fig. B-1. For the problem to be worked, the expressions corresponding to the flow diagram are punched on IBM cards and are then placed into the computer, along with the punched paper tape. The computer will then solve the problem and print the output.

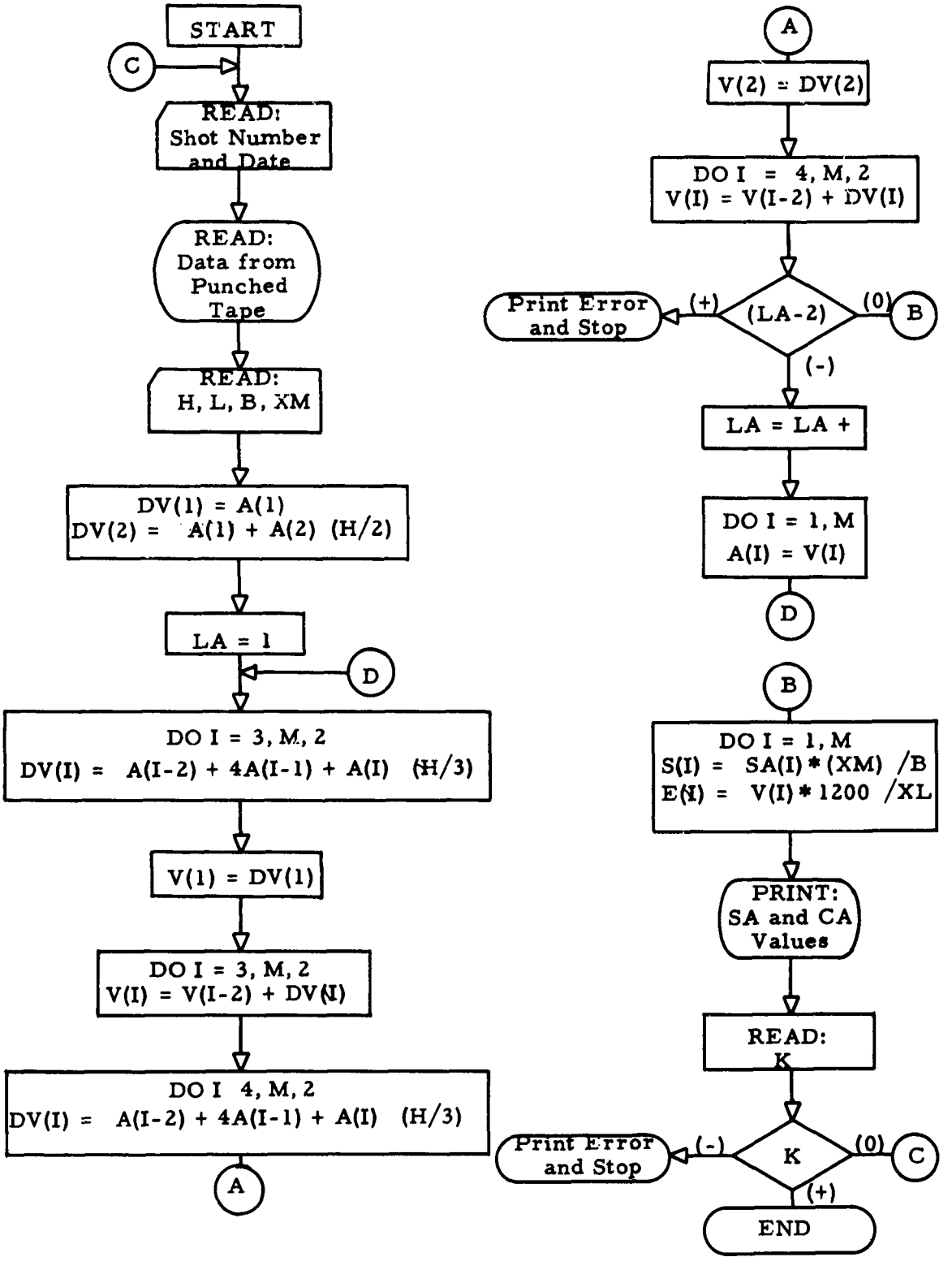


Fig. B-1. Flow Diagram for Conversion of Acceleration-Time Curves to Stress-Strain Data Using a Digital Computer.

# APPENDIX C

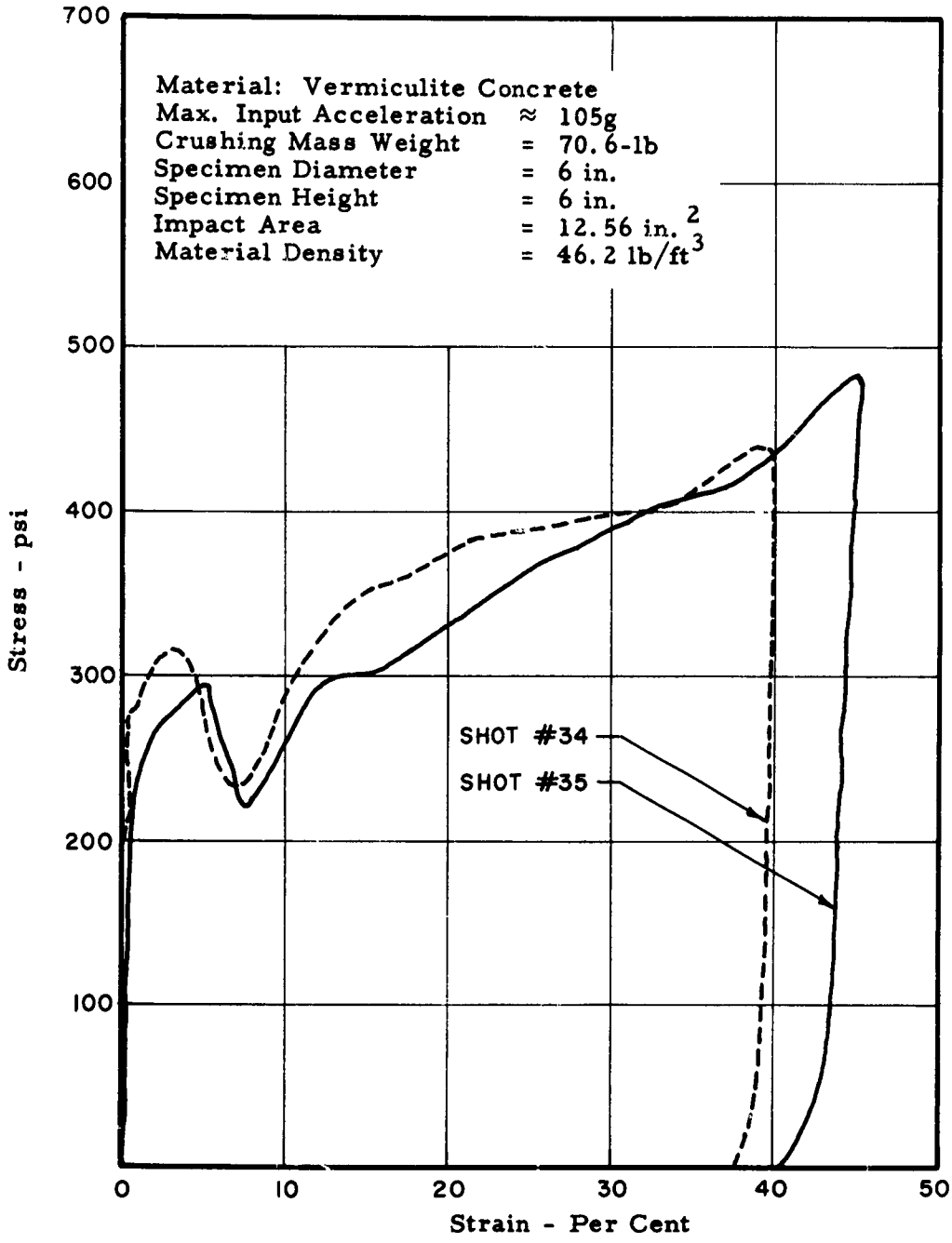


Fig. C-1. Stress-Strain Curves for Vermiculite Concrete, Shots No. 34 and 35.

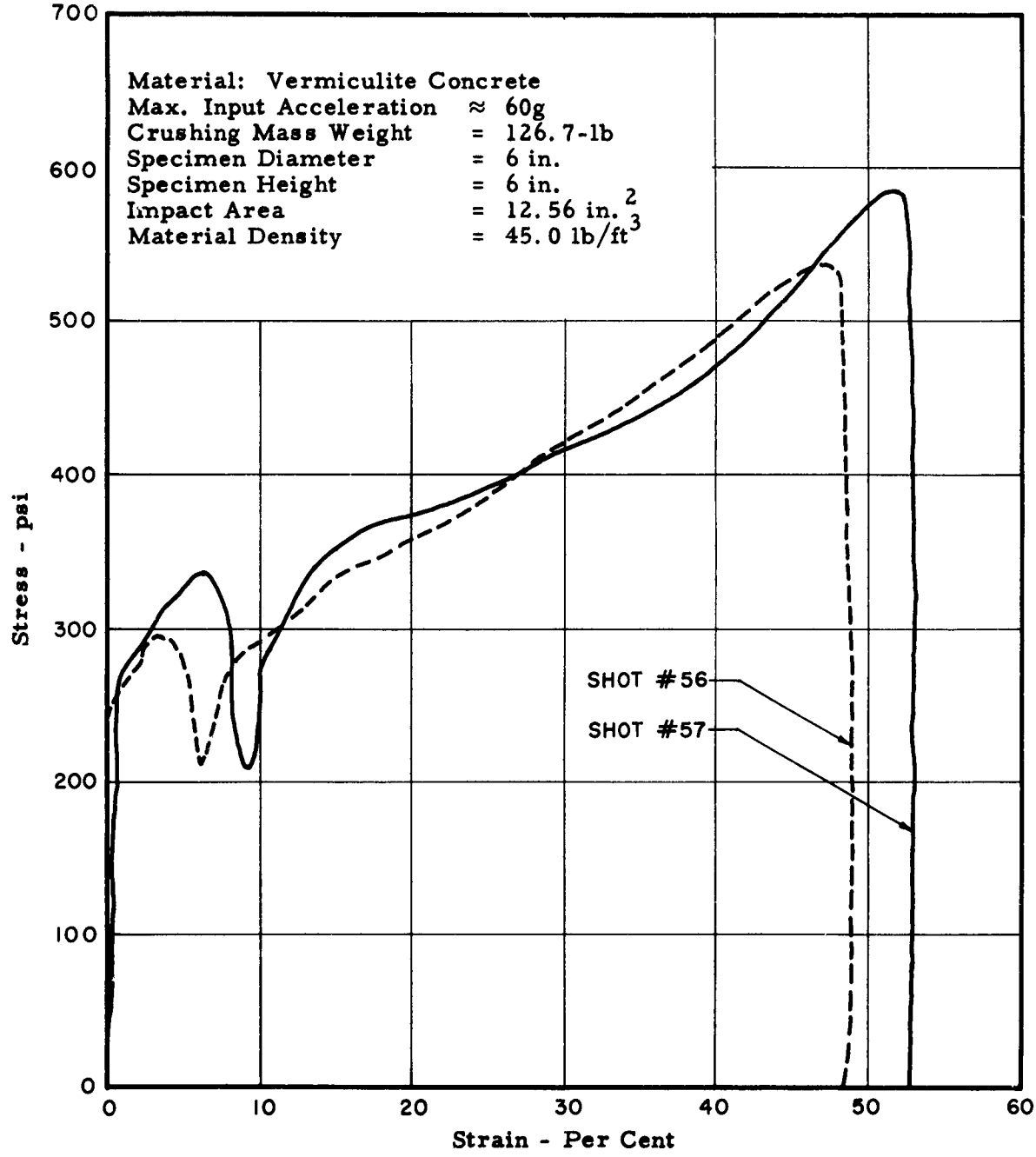


Fig. C-2. Stress-Strain Curves for Vermiculite Concrete, Shots No. 56 and 57.

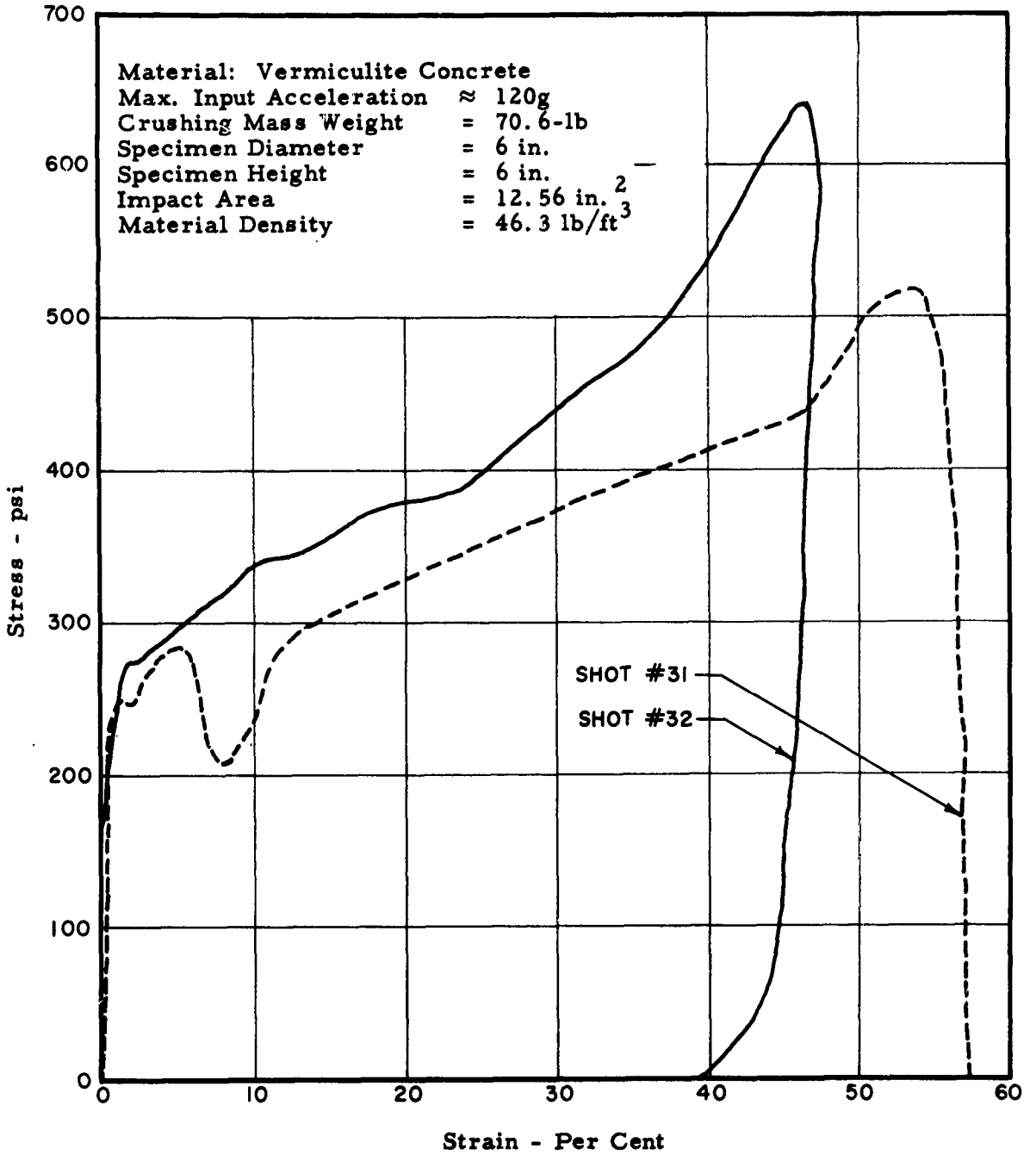


Fig. C-3. Stress-Strain Curves for Vermiculite Concrete, Shots No. 31 and 32.

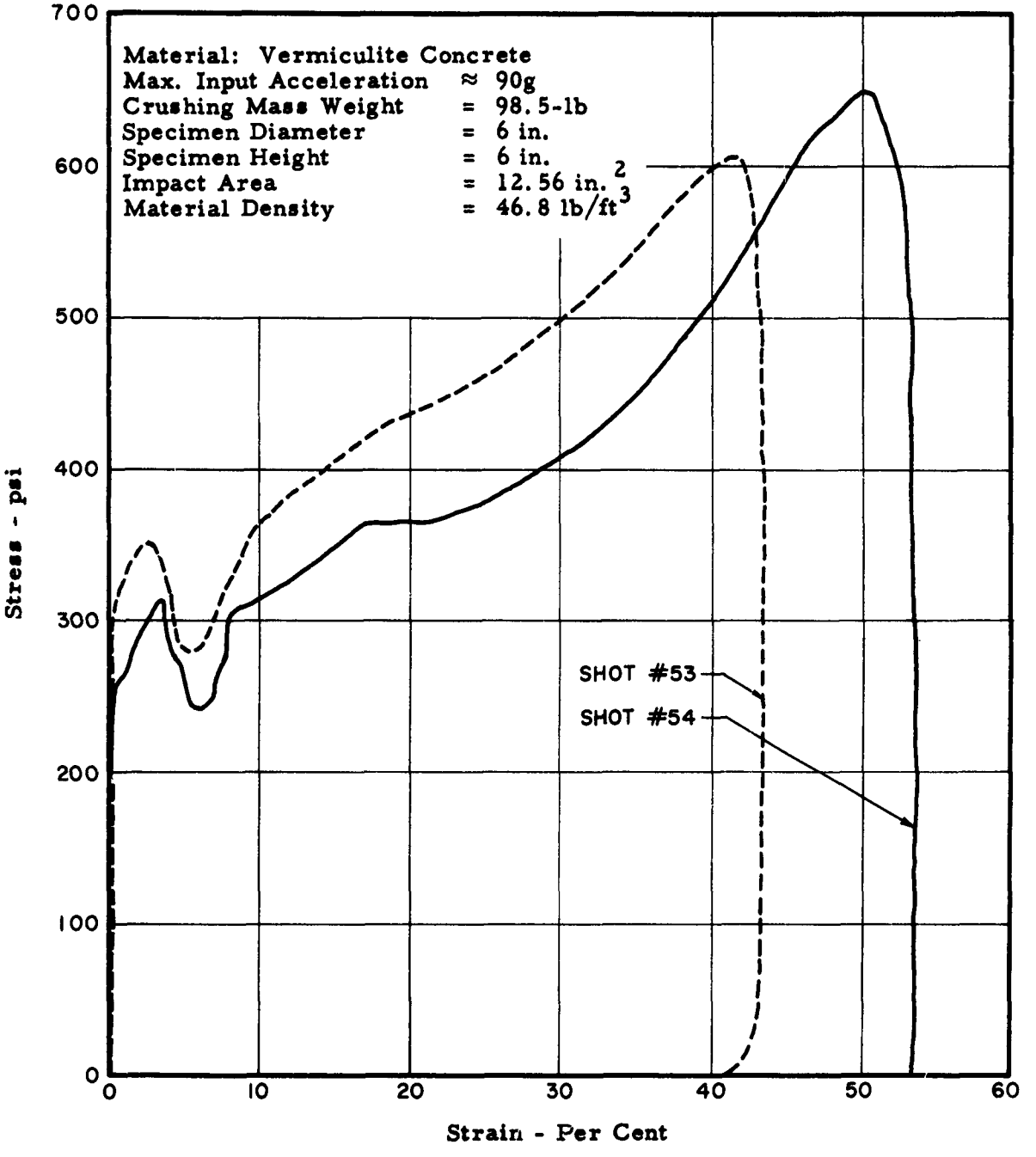


Fig. C-4. Stress-Strain Curves for Vermiculite Concrete, Shots No. 53 and 54.

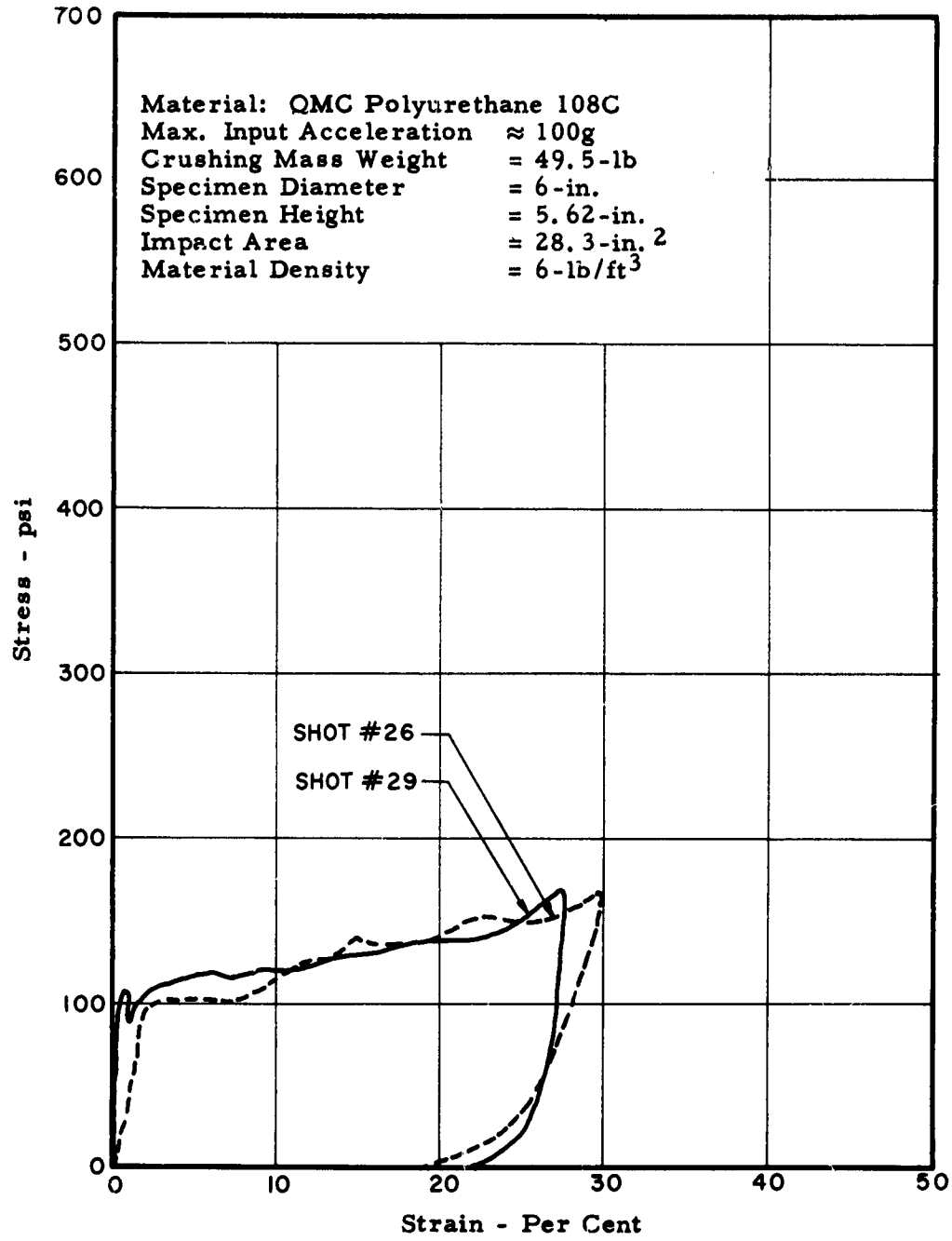


Fig. C-5. Stress-Strain Curves for Foamed Plastic, Shots No. 26 and 29.

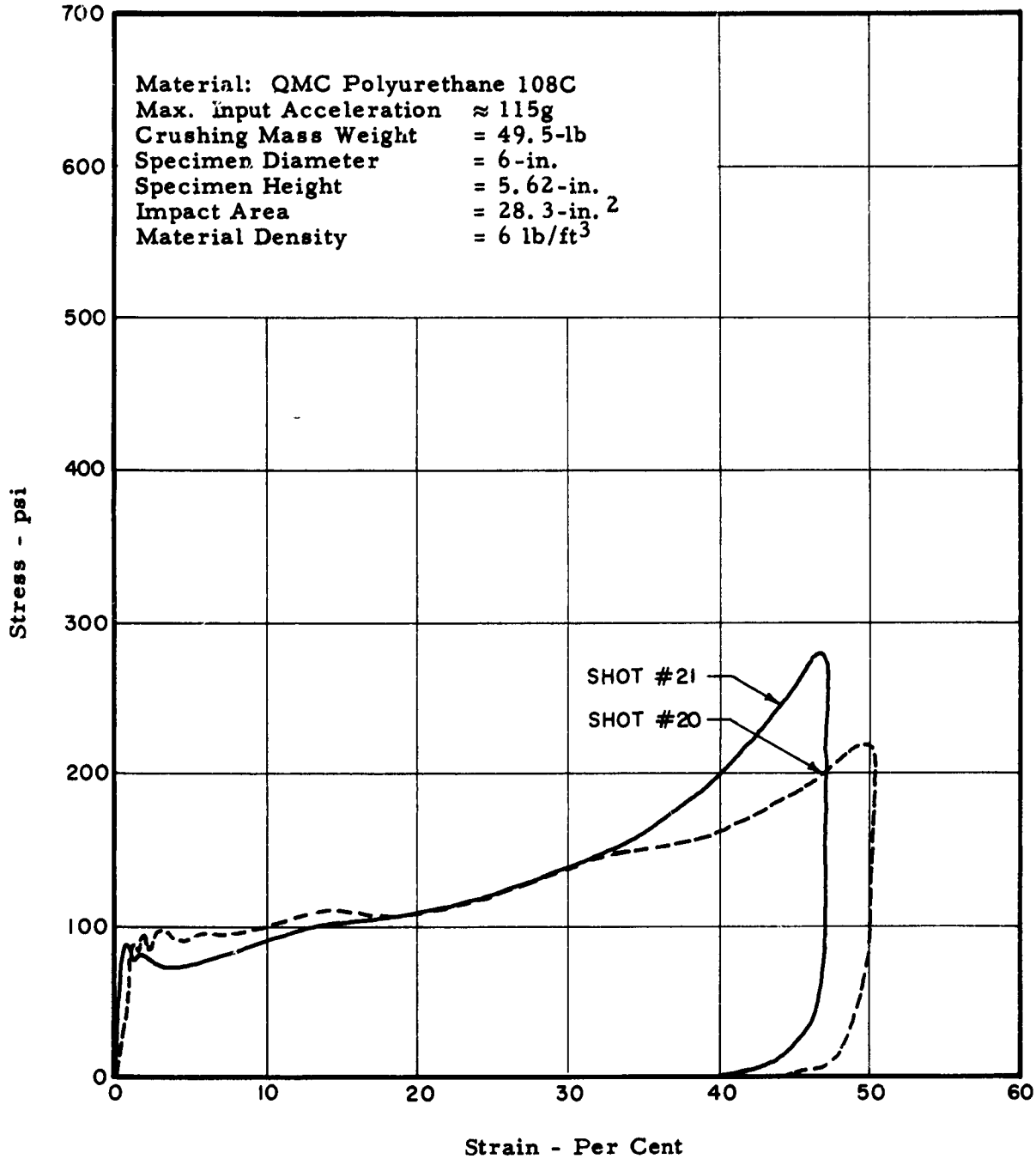


Fig. C-6. Stress-Strain Curves for Foamed Plastic, Shots No. 20 and 21.

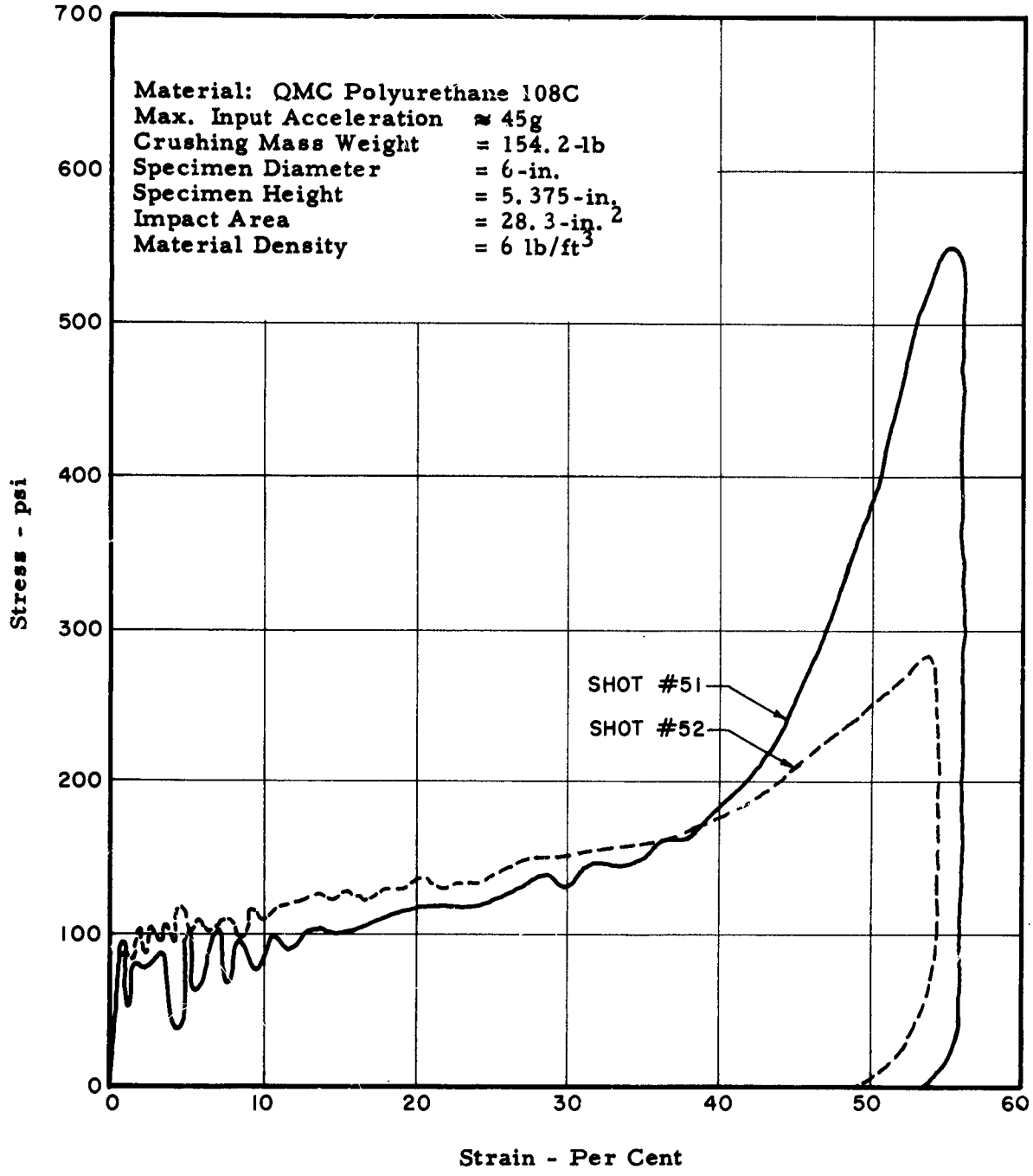


Fig. C-7. Stress-Strain Curves for Foamed Plastic, Shots No. 51 and 52.

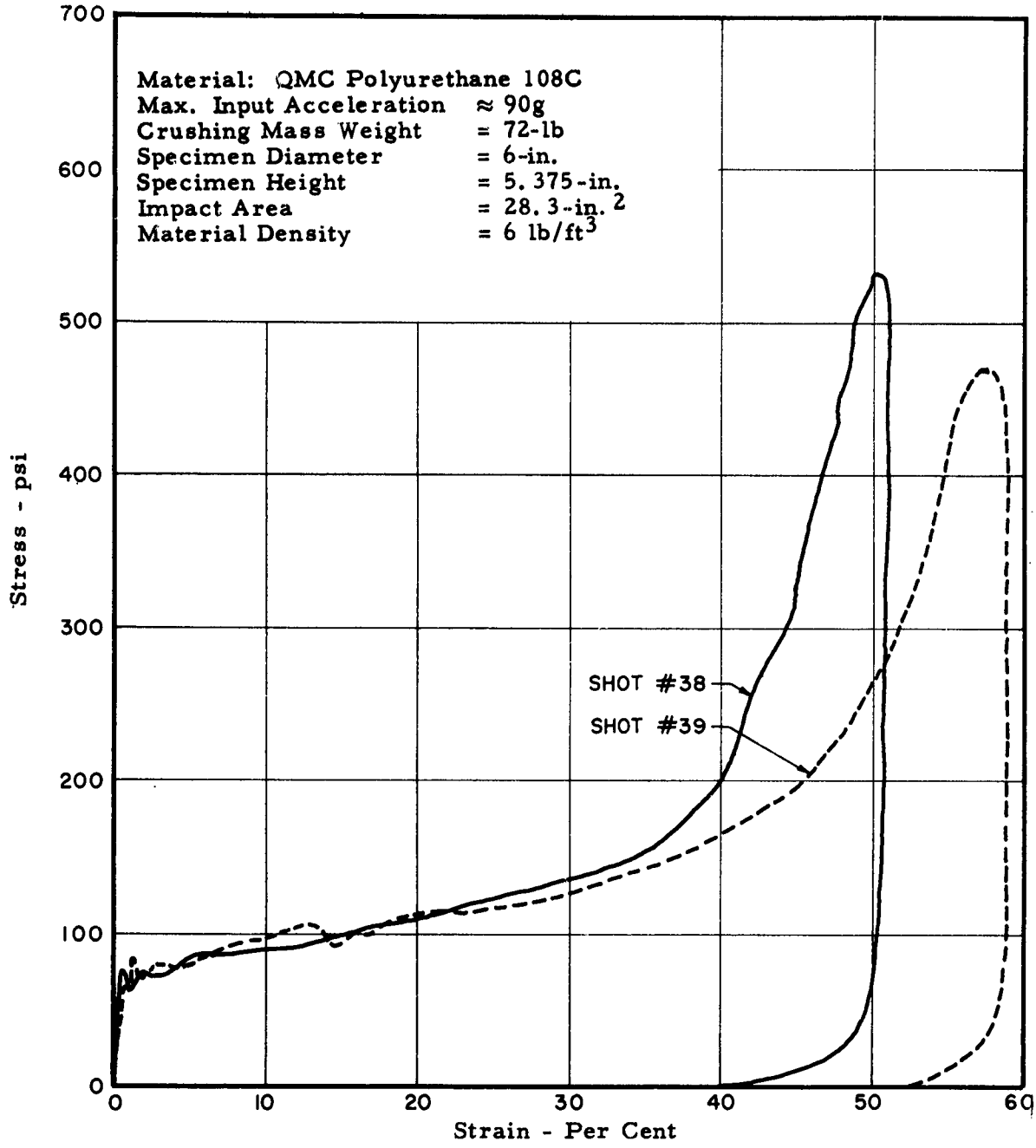


Fig. C-8. Stress-Strain Curves for Foamed Plastic, Shots No. 38 and 39.

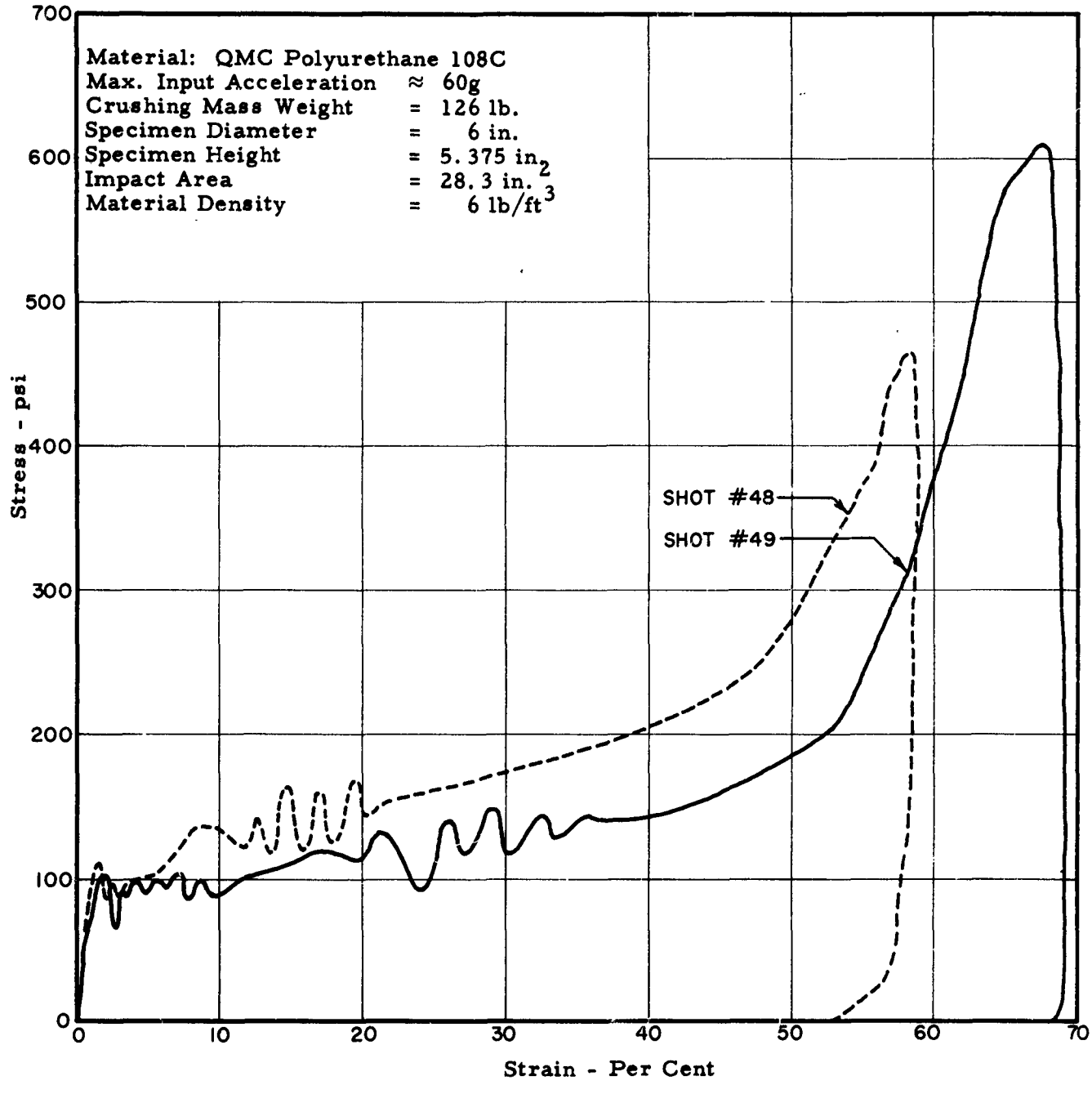


Fig. C-9. Stress-Strain Curves for Foamed Plastic, Shots No. 48 and 49.

# DISTRIBUTION LIST

## ARMY

| ADDRESSEE | NO. OF CYS |
|---|---|
| Chief of Engineers, DA, Washington 25, D. C., ATTN: ENGNB<br>ATTN: ENGEB | 1 |
| Commanding General, U. S. Continental Army Command, Ft. Monroe, Va. | 1 |
| President, U. S. Army Air Defense Board, Ft. Bliss, Texas | 1 |
| Commandant, Command & General Staff College, Ft. Leavenworth, Kansas, ATTN: Archives | 1 |
| Director, Special Weapons Development, Hq CONARC, Ft. Bliss, Texas, ATTN: Chester I. Peterson | 1 |
| Commanding General, U. S. Army Chemical Corps, R&D Command, Washington 25, D. C. | 1 |
| Commanding General, Aberdeen Proving Ground, Aberdeen, Md., ATTN: Director, BRL | 1 |
| Commanding General, The Engineer Center, Ft. Belvoir, Va., ATTN: Asst Commandant, Engineer School | 1 |
| Commanding Officer, Engineer Research & Development Lab., Ft. Belvoir, Va., ATTN: Chief, Tech Support Branch | 1 |
| Commanding Officer, USA Signal R&D Lab, Ft. Monmouth, N. J., ATTN: Technical Documents Center, Evans Area | 1 |
| Commanding Officer, Chemical Warfare Lab., Army Chemical Center, Md., ATTN: Tech Library | 1 |
| Director, Waterways Experiment Station, P. O. Box 631, Vicksburg, Miss., ATTN: Library | 1 |
| The Research and Analysis Corporation, 6935 Arlington Rd., Bethesda Md., Washington 14, D. C. | 1 |

## NAVY

| | |
|---|---|
| Director of Naval Intelligence, DN, Wash 25, D. C., ATTN: OP-922V | 1 |
| Chief, Bureau of Naval Weapons, DN, Washington 25, D. C. | 2 |

## DISTRIBUTION LIST

(Cont'd)

| ADDRESSEE | NO. OF CYS |
|---|---|
| Chief, Bureau of Yards & Docks, DN, Wash 25, D. C., ATTN: D-400 | 1 |
| ATTN: D-440 | 1 |
| Chief of Naval Research, DN, Wash 25, D. C., ATTN: Code 811 | 1 |
| Superintendent, U. S. Naval Postgraduate School, Monterey, Calif. | 1 |
| Commanding Officer, Nuclear Weapons Training Center, Atlantic, Naval Base, Norfolk 11, Va., ATTN: Nuclear Warfare Dept. | 1 |
| Commanding Officer, U.S. Naval Schools Command, U.S. Naval Station, Treasure Island, San Francisco, Calif. | 1 |
| Commanding Officer, Nuclear Weapons Training Center, Pacific, Naval Station, North Island, San Diego 35, Calif. | 2 |
| Commanding Officer, U.S. Naval Damage Control Training Center, Naval Base, Philadelphia 12, Pa., ATTN: ABC Defense Course | 1 |
| Commander, U. S. Naval Ordnance Lab., White Oak, Silver Spring, Md. | |
| ATTN: EA | 1 |
| ATTN: EU | 1 |
| ATTN: E | 1 |
| Commander, U. S. Naval Ordnance Test Station, China Lake, Calif. | 1 |
| Commanding Officer & Director, U.S. Naval Civil Engineering Lab., Port Hueneme, Calif., ATTN: Code L31 | 1 |
| Director, U.S. Naval Research Lab., Washington 25, D. C. | 1 |
| Commanding Officer & Director, Naval Electronics Lab., San Diego 52, Calif. | |
| Commanding Officer, U.S. Naval Radiological Defense Laboratory, San Francisco, Calif., ATTN: Tech Info Division | 1 |
| Commander, Norfolk Naval Shipyard, Portsmouth, Va., ATTN: Underwater Explosions Research Division | 1 |

### AIR FORCE

| | |
|---|---|
| Air Force Intelligence Center, Hq USAF, ACS/I (AFCIN-3VI), Wash 25, D. C. | 1 |
| Commander-in-Chief, Strategic Air Command, Offutt AFB, Nebraska, ATTN: OAWS | 1 |

## DISTRIBUTION LIST

(Cont'd)

| ADDRESSEE | NO. OF CYS |
|---|---|
| Commander, Air Material Command, Wright-Patterson AFB, Ohio | 2 |
| Commander, Air Research & Development Command, Andrews AFB, Wash 25, D. C., ATTN: RDRWA | 1 |
| Director, Air University Library, Maxwell AFB, Alabama | 2 |
| Commander, AF Cambridge Research Center, L. G. Hanscom Field, Bedford, Mass., ATTN: CRQST-2 | 1 |
| Commander, AF Special Weapons Center, Kirtland AFB, New Mexico, ATTN: Tech Info Office | 1 |
| Commandant, USAF Institute of Technology, Wright-Patterson AFB, Ohio, ATTN: MCLI-ITRIDL | 1 |
| Commander, Western Development Division (ARDC), P. O. Box 262, Inglewood, Calif. | 1 |
| Director, USAF Project RAND, Via: U. S. Air Force Liaison Office, The RAND Corporation, 1700 Main Street, Santa Monica, Calif. | 1 |
| Director of Civil Engineering, Hq USAF, Washington 25, D. C., ATTN: AFOCE | 1 |
| **OTHERS** | |
| Director of Defense Research & Engineering, Wash 25, D. C., ATTN: Tech Library | 1 |
| U. S. Documents Officer, Office of the United States National Military Representative-SHAPE, APO 55, New York, N. Y. | 1 |
| Director, Weapons Systems Evaluation Group, OSD, Room 1E880, The Pentagon, Washington 25, D. C. | 1 |
| Commandant, Armed Forces Staff College, Norfolk 11, Va., ATTN: Library | 1 |
| Commander, Field Command, DASA, Sandia Base, Albuquerque, New Mexico | 5 |
| Commander, Field Command, DASA, Sandia Base, Albuquerque, New Mexico, ATTN: Training Division | 2 |
| Chief, Defense Atomic Support Agency, Washington 25, D. C. | 5 |

## DISTRIBUTION LIST

(Cont'd)

| ADDRESSEE | NO. OF CYS |
|---|---|
| Chief, Defense Atomic Support Agency, Washington 25, D. C., ATTN: Major Vickery | 2 |
| Commandant, Army War College, Carlisle Barracks, Pa., ATTN: Library | 1 |
| Commandant, National War College, Washington 25, D. C., ATTN: Class Rec Library | 1 |
| Commandant, The Industrial College of the Armed Forces, Ft. McNair, Washington 25, D. C. | 1 |
| Officer-in-Charge, US Naval School, Civil Engineering Corps Officers, US Naval Construction Battalion, Port Hueneme, Calif. | 1 |
| Los Alamos Scientific Laboratory, P. O. Box 1663, Los Alamos, New Mexico, ATTN: Report Librarian (For Dr. Alvin C. Graves) | 1 |
| Administrator, National Aeronautics & Space Administration, 1512 "H" Street N. W., Washington 25, D. C. | 1 |
| Langley Research Center, NASA, Langley Field, Hampton, Va., ATTN: Mr. John Stack | 1 |
| Chief, Classified Technical Library, Technical Information Service, U. S. Atomic Energy Commission, Washington 25, D. C., ATTN: Mrs. Jean O'Leary | 1 |
| Manager, Albuquerque Operations Office, U. S. Atomic Energy Commission, P. O. Box 5400, Albuquerque, New Mexico | 1 |
| Dr. Robert J. Hansen, Division of Industrial Cooperation, Massachusetts Institute of Technology, 77 Massachusetts Ave., Cambridge, Mass., | 1 |
| Dr. Bruce G. Johnston, The University of Michigan, University Research Security Office, Lobby 1, East Engineering Bldg, Ann Arbor, Michigan | 1 |
| Sandia Corporation, Sandia Base, Albuquerque, New Mexico, ATTN: Classified Document Division (For M. L. Merritt) | 1 |
| Superintendent, Eastern Experiment Station, U. S. Bureau of Mines, College Park, Md., ATTN: Dr. Leonard Obert | 1 |
| Dr. Nathan M. Newmark, University of Illinois, Room 207, Talbot Lab., Urbana, Illinois | 1 |
| Commander, ASTIA, Arlington Hall Station, Arlington 12, Va., ATTN: TIPDR | 20 |

## DISTRIBUTION LIST

(Cont'd)

| ADDRESSEE | NO. OF CYS |
|---|---|
| Holmes & Narver Inc., AEC Facilities Division, 849 S. Broadway, Los Angeles 14, Calif., ATTN: Mr. Frank C. Galbreth | 1 |
| American Machine and Foundry, 7501 North Natchez Avenue, Niles, Illinois | 1 |
| Southwest Research Institute, 8500 Culebra Road, San Antonio 6, Texas | 1 |
| Armour Research Foundation, 10 West 35th Street, Chicago 16, Illinois | 1 |
| Barry Wright Corporation, 700 Pleasant Street, Watertown 72, Massachusetts | 1 |
| Roland F. Beers, Inc., P. O. Box 23, Alexandria, Virginia ATTN: Mr. Sherwood B. Smith | 1 |
| Iowa State University, Ames, Iowa | 1 |
| NESCO, 711 South Fair Oaks Avenue, Pasadena, California | 1 |
| Engineering-Physics Company, 5515 Randolph Road, Rockville, Maryland | 1 |